

Reviewed Preprint

v1 • May 6, 2026

Not revised

✉ For correspondence:

c.t.schafer@vu.nl

* BdB, TDL, and KV contributed equally to the work.

Competing interests: No competing interests declared

Funding: See [page 21](#)

Reviewing editor: Nevin A Lambert, Augusta University, United States

© 2026, de Boer et al. This article is distributed under the terms of the [Creative Commons Attribution License](#), which permits unrestricted use and redistribution provided that the original author and source are credited.

Selective suppression and biasing of chemokine receptors CCR9 and ACKR4 through targeting CCL25 with de novo miniproteins

Bas de Boer*, Thomas D Lamme*, Karlijn Verdwaald*, Sara Santamaria Medina, Csongor G Németh, Elisabeth M Elfrink, Martine J Smit, Iwan JP de Esch, Christopher T Schafer ✉

Faculty of Science, Department of Chemistry and Pharmaceutical Sciences, Division of Medicinal Chemistry, Amsterdam Institute for Molecular and Life Sciences (AIMMS), Vrije Universiteit Amsterdam, Amsterdam, Netherlands

eLife Assessment

This **important** study describes computationally designed proteins that bind to the chemokine CCL25. The authors present evidence that some binders simply prevent chemokine binding to the CCR9 receptor, while one binder changes the downstream signaling triggered by chemokine binding. The evidence is **solid** overall, but some uncertainty remains with respect to functional selectivity due to sensitivity differences between functional assays and the degree of binder selectivity between the large family of chemokine ligands.

<https://doi.org/10.7554/eLife.111190.1.sa4>

Abstract

Chemokines and their receptors mediate cell migration and coordinate immune responses, while dysregulation can lead to inflammation. Therapeutic modulation of the chemokine signaling axis has proven difficult. Most drug discovery efforts target the receptors, whereas natural regulatory mechanisms focus on the chemokines. Despite this insight, development of effective chemokine-directed modulators has remained elusive. Recent advances in de novo protein design offer an unprecedented opportunity to produce high-affinity binders that efficiently block protein-protein interactions. We implemented a computational workflow leveraging the BindCraft platform to generate miniprotein binders against CCL25, the chemokine ligand for the receptors CCR9 and ACKR4 and implicated in inflammatory bowel diseases. The unbiased development results in several miniproteins designed to block the receptor N-terminus from wrapping the chemokine and prevent productive engagement. Thus, these proteins suppress CCL25-mediated effector coupling and halt MOLT-4 lymphoblast migration. Another class of miniprotein, represented by VUP25111, is predicted to bind CCL25 along the chemokine β 1 strand and retained receptor binding. This complex inhibited arrestin recruitment to CCR9, but not to ACKR4, indicating receptor specificity. Additionally, G protein signaling through CCR9 was unimpeded by VUP25111, suggesting that the miniprotein biased the native balanced agonist towards G proteins. These results demonstrate the effectiveness of differentially targeting CCL25 to suppress CCR9 signaling and new tools to resolve the structural basis of chemokine receptor activation and bias.

Introduction

Chemokines are small secreted proteins (~10 kDa) that direct cell migration throughout the body by activating chemokine receptors, a subfamily of G protein-coupled receptors (GPCRs). The chemokine system plays critical roles in coordinating immune responses and homeostasis, as well as directing cell positioning during development and wound repair [1]. Dysregulation of either the

receptors or chemokines results in inflammatory diseases, cancer metastasis, and immune evasion of cancers and pathogens [2]. While attractive therapeutic GPCR targets, it has proven difficult to develop effective drugs towards chemokine receptors and only a few candidates have reached the clinic. This suggests that new targeting strategies are needed to fully exploit this versatile and promising signaling pathway [3,4].

The receptor:chemokine system comprises ~50 chemokines and ~20 receptors, forming an intricate web of cross-reactivity that allows for highly specific cell positioning [5]. Chemokine binding to chemokine receptors is often simplified to a two-site, two-step model, predominantly involving contacts with the receptor N-terminus and the orthosteric ligand-binding site in the transmembrane (TM) domain, termed chemokine recognition site (CRS) 1 and 2, respectively (Fig. 1A) [6–8]. Early models proposed that CRS1 would catch the chemokines and orient binding into CRS2 for receptor activation. Subsequent studies suggested that the ligands interact first with the TM domain of CRS2, and the N-terminus follows by wrapping around the chemokine to stabilize a higher affinity state [9]. Both sites are generally required for activation, with N-terminal receptor truncations or CRS2 point mutations being equally effective at impairing signaling responses [9–12]. Proper binding leads to GPCR activation and coupling of G protein and/or arrestin effector proteins.

The CC chemokine receptor 9 (CCR9) is expressed on thymocytes and intestinal lymphocytes [13,14] and promotes the migration of immune cells between the thymus and small intestine in response to its sole native agonist, CC chemokine CCL25 [15,16]. This receptor:chemokine pair regulates T cell development in the thymus and coordinates immune homeostasis and surveillance in the colon. Thus, overexpression and imbalance of this signaling axis are implicated in inflammatory bowel (IBD) and Crohn's diseases [17,18], as well as contributing to cancer metastasis to the gut [19,20]. Clinical development of CCR9 antagonists has thus far been unsuccessful, with efficacy in patients remaining a significant challenge [21].

Biological interference of the receptor:chemokine axis preferentially occurs at the level of the chemokine rather than the receptors. For example, pathogens and pests modulate immune responses targeting chemokines. To avoid the host's immune response, ticks have evolved small, salivary chemokine-binding proteins called evasins that block the chemokine interactions with receptors or glycosaminoglycans [22,23]. This action prevents the immune system from responding and impeding the tick's blood meal. Another, perhaps more cumbersome, way to target chemokines is by atypical chemokine receptors (ACKRs) that scavenge chemokines by internalizing the receptor:chemokine complex into the cell, thereby altering the chemokine gradients that are essential for chemokine-driven cell migration [24]. For example, CCL25 is an agonist for CCR9 but is scavenged by the atypical chemokine receptor ACKR4 [25]. These examples suggest that targeting the chemokine ligand may represent an effective mechanism for remodeling immune responses.

To study the chemokine receptor:chemokine axis in more detail, a variety of chemokine modulators is needed. However, these small proteins have proven challenging to target effectively using conventional approaches. For example, an NMR-based CCL28 fragment screen gave a low hit rate (<1%) of very weak affinity binders ($K_d > 1$ mM) [26], thereby indicating low ligandability. We were therefore prompted to consider alternative approaches. With an avalanche of protein structural information becoming available, the use of de novo structure generation algorithms is making a revival. Recent advances in artificial intelligence-driven structure prediction have yielded highly accurate tools such as AlphaFold2 (AF2) [27]. Building on these developments, researchers have introduced de novo binder design frameworks that generate protein structures and sequences from scratch [28], including Chai-2 [29], AlphaProteo [30], and BindCraft [31]. The latter has emerged as a fully integrated, one-shot platform for binder design based only on an input target protein. BindCraft is an AF2-driven inverse-design pipeline that hallucinates binder sequences by backpropagating gradients through AlphaFold2-Multimer [32] and repredicting the binder-target complex at every iteration, enabling flexible co-optimization of sequence, structure, and interface. Designed binders are further refined using MPNNsol [33] and filtered based on AF2

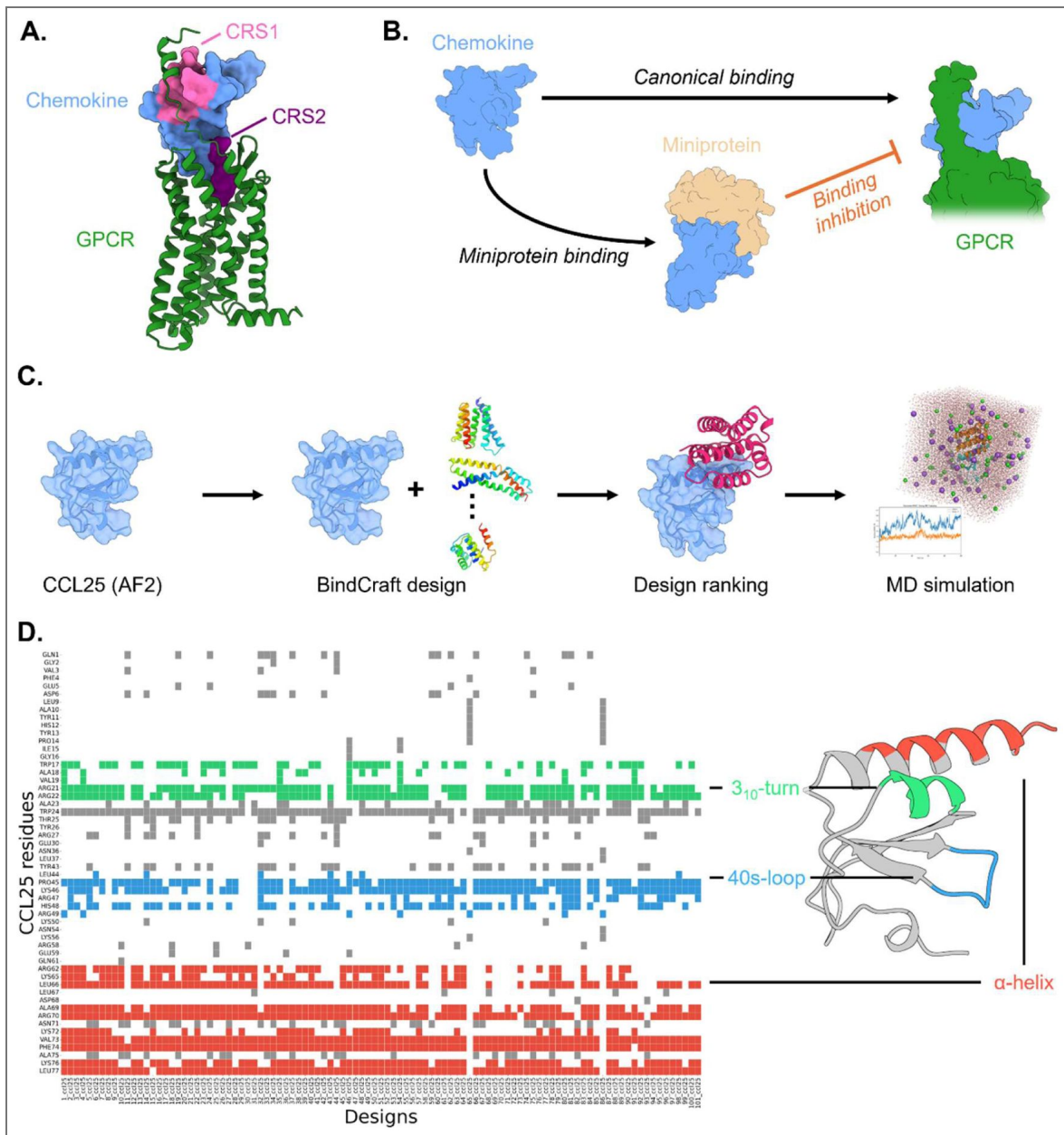


Figure 1. Design strategy and computational workflow for miniprotein binder design against CCL25.

(A) Chemokine interacts with chemokine receptors primarily through CRS1 (Pink, receptor N-terminus with chemokine body) and CRS2 (Purple, chemokine N-terminus with receptor TM domain). The receptor:chemokine complex is generated using AF3 with sequences of CCR9 and CCL25. (B) Conceptual framework illustrating the strategy for inhibiting canonical chemokine to receptor binding by directly targeting chemokine with designer miniprotein binders. (C) Computational workflow used to generate chemokine-binding miniproteins. (D) Molecular interaction map summarizing contacts between all miniprotein designs and CCL25. The most frequently targeted structural elements, the α -helix, the 3_{10} -turn, and the 40s-loop, are highlighted in red, green, and blue, respectively.

confidence and Rosetta [34] physics-based metrics. The platform's integrated workflow makes BindCraft easy to apply, lowering the barrier of entry for *de novo* binder design and enabling broad accessibility with a high success rate against a diverse set of targets [31,35,36].

Here, we apply BindCraft's *de novo* protein design to generate modulators for CCL25. Out of the generated BindCraft designs, four miniproteins were selected, produced, isolated and characterized. All show selective binding to CCL25 and form complexes that inhibit receptor activation. Most prevent activation by impeding chemokine binding to the receptor, thus impairing all signaling and migratory responses, but one forms a G protein-biased complex with CCL25 and selectively inhibits CCR9, but not ACKR4. These results highlight the effectiveness of targeting chemokines with *de novo* protein modulators as unique research tools to probe the receptor:chemokine signaling axis.

Results

Generation of *de novo* miniprotein binders targeting CCL25

In order to generate binders against CCL25, the AF2-predicted model was obtained from the AlphaFold protein database [37]. CCL25 is the largest member of the chemokine family and contains a long C-terminal extension following the classic chemokine fold. To focus the miniprotein designs on the core chemokine domain to block CRS interactions and receptor binding (Fig. 1A, B), we performed our design efforts using a truncated form of the chemokine. The truncated CCL25 (CCL25_ΔCT, 1-77) activated both CCR9 and ACKR4 with similar potency and efficacy as the full-length ligand (Fig. S1).

The overall workflow is presented in Fig. 1C. Starting from the CCL25 AlphaFold2 model, the BindCraft algorithm generates candidate designs of 75-125 amino acids with diverse structures. No predefined binding hotspots were imposed, and thus, designs were permitted to explore the entire CCL25 surface, allowing BindCraft to identify favorable interaction sites. At most two proteins with identical backbones were used for further processing to promote diversity among the designed binders. Following the design run, after 101 candidates passed computational filters, binders were ranked by the ipTM score. Predicted complexes demonstrated robust prediction metrics, with ipTM scores (interface predicted TM-score) ranging from 0.55 to 0.87, ipAE scores (interface predicted aligned error) from 0.16 to 0.34, and pLDDT scores (predicted local distance difference test) from 0.83 to 0.95 (Fig. S2). Structural inspection revealed substantial backbone diversity among designs, although all adopted predominantly α -helical secondary structures (Fig. S3). Pairwise TM-score analysis yielded an average of 0.41, and UMAP projection of TM-score similarities confirmed broad structural dispersion (Fig. S3). Despite the absence of a predefined binding hotspot, most designs target a region encompassing one face of the α -helix, the 3_{10} -turn, and the 40s-loop with large structural diversity (Fig. 1D). As a last step, we subjected the top 20 miniprotein designs to 100 ns MD simulations to assess complex stability. Calculation of the backbone RMSD of the binders reveals good stability for all complexes, and estimation of binding free energy using the MM/GBSA method [38] furthermore predicts favorable binding complexes of all top 20 miniproteins (Table S1).

De novo designed binders target CCL25 with high affinity

From the top 20 scored binders, four were selected for insertion into expression vectors for *E. coli* purification based on predicted binding energies, diversity of structural scaffolds, and binding interfaces (Fig. 2A, Table S1). Three of the four VU miniproteins (VUPs), VUP25101, VUP25107, and VUP25112, are predicted to interact with the C-terminal helix of the chemokine, blocking CRS1, opposite the GPCR transmembrane bundle. The fourth, VUP25111, makes unique interactions compared to the others (Fig. S4) and is predicted to bind along the β 1 strand and 40s-loop of CCL25 without substantially impairing either CRS1 or CRS2 binding interfaces. The binding of the designed miniproteins to CCL25 was validated by fluorescence polarization spectroscopy (FP) of a fluorophore (AZ488) attached to the C-terminus of full-length CCL25. An increase in the polarization of the fluorophore emission is the result of a decrease in the tumbling rate during

fluorophore excitation and is reflective of an increase in the size of the protein complex due to miniprotein binding (Fig. 2B). All four tested binders produced an increase in polarization, indicating that the miniproteins indeed bind the CCL25 target (Fig. 2C). Similar affinity values were calculated for all four VUPs (VUP25101: $pK_d = 6.42 \pm 0.74$, VUP25107: $pK_d = 6.82 \pm 0.43$, VUP2525111: $pK_d = 6.36 \pm 0.35$, VUP25112: $pK_d = 6.30 \pm 0.41$). Importantly, these results also confirm that the miniproteins bind the full-length CCL25 chemokine despite being designed against an artificially truncated form, CCL25_ΔCT.

Miniproteins block CCL25 binding to CCR9 and ACKR4

As the miniproteins designed against CCL25 bind the desired chemokine in purified form, we next determined whether the CCL25-miniprotein complex inhibits binding to the receptor as intended. Binding of CCL25 to CCR9 or ACKR4 was determined by Time-Resolved Fluorescence Resonance Energy Transfer (TR-FRET) between a lanthanide donor attached to a snap tag fused to the receptor N-terminus and a fluorophore on the C-terminus of CCL25 (AZ647) (Fig. 3A). CCL25_ΔCT was used in place of the full-length chemokine to shorten the distance between the donor and acceptor and improve energy transfer efficiency. Incubating CCL25 with three of the miniproteins, VUP25101, VUP25107, and VUP25112, impaired binding to both CCR9 and ACKR4 and resulted in a complete loss of FRET at high miniprotein concentration (Fig. 3B, C), thereby demonstrating that these molecules act as potent inhibitors by directly interfering with CCL25 binding to the receptors. In the case of VUP25111, only the highest tested concentrations decreased CCL25 binding to either receptor, but did not completely eliminate the binding signal. Since the binder readily complexes with the chemokine at these concentrations (Fig. 2), this suggests that CCL25:VUP25111 may bind the receptors cooperatively.

To explore a possible structural explanation for how the binders prevent CCL25 from engaging its receptors, we modeled the CCR9:CCL25 and ACKR4:CCL25 complexes using AlphaFold3 [39]. Superimposing the VUP25101:CCL25 complex onto the predicted receptor:chemokine complexes shows steric clashes in CRS1 between the miniprotein and the N-terminus of both CCR9 and ACKR4 (Fig. 3D). This suggests that disrupting solely these contacts is sufficient to block proper receptor:chemokine complex formation. In contrast, superimposing the VUP25111:CCL25 complex on the models shows only minor clashes with the extracellular loop 2 (ECL2) of CCR9 and no predicted conflicts with ACKR4. Together, these results indicate that blocking CRS1 interactions between the receptor N-terminus and chemokine body robustly prevents CCL25 binding to both its canonical and atypical receptors, while targeting the β1-strand appears structurally tolerated.

De novo miniproteins selectively inhibit CCL25-mediated arrestin recruitment to CCR9 and ACKR4

The effect of CCL25-targeting on receptor activation was first evaluated by assessing arrestin recruitment. Both CCR9 and ACKR4 show robust engagement with arrestins following agonist stimulation and serve as simple readouts of changes in receptor activation [40,41]. Thus, β-arrestin2 recruitment to the receptors was measured by BRET between a C-terminal luciferase fusion on the receptor (RlucII) and an N-terminal GFP10 on β-arrestin2 (Fig. 4A). In both cases, the addition of chemokine leads to a substantial increase in resonance energy transfer, indicating translocation of the effector in response to agonist-mediated receptor activation (Fig. 4B, C). Adding an increasing concentration of the miniprotein binders with a constant 20 nM CCL25 (Full-Length) progressively decreased the CCL25-promoted activation and all binders completely inhibited CCR9-arrestin recruitment at the highest concentrations (Fig. 4B). VUP25101, VUP25107, and VUP25112 showed similarly effective suppression of CCL25-mediated activation of CCR9 (VUP25101: $pIC_{50} = 7.92 \pm 0.07$; VUP25107: $pIC_{50} = 8.01 \pm 0.24$; VUP25112: $pIC_{50} = 7.56 \pm 0.41$). The IC_{50} of VUP25111 was dramatically shifted by 2 log units ($pIC_{50} = 5.77 \pm 0.33$). Given the different binding mode of VUP25111 to CCL25 (Fig. 3D), this indicates that the mechanism by which VUP25111 inhibits CCR9 activation may also differ. Specificity for the CCL25 system was

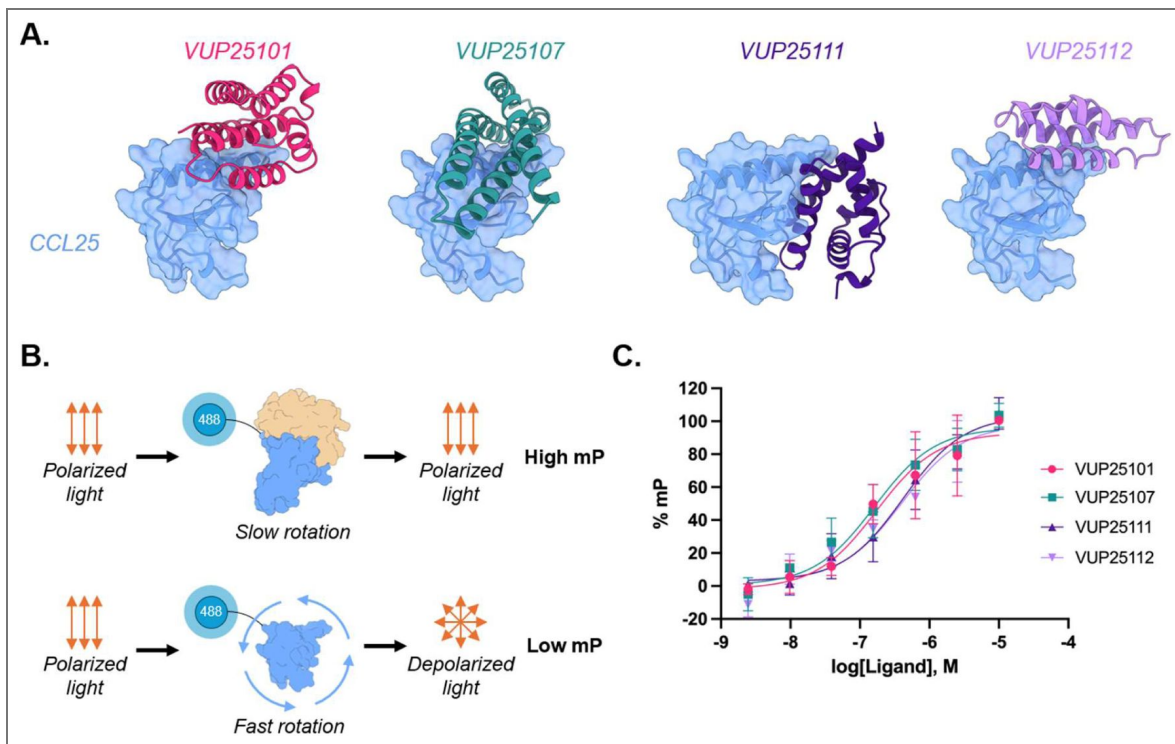


Figure 2. VUPs (VU miniproteins) are confirmed to directly bind CCL25.

(A) Structural models of the generated designs for CCL25. CCL25 is shown in blue with a surface representation, and the binders are displayed as cartoon in various colors. (B) Cartoon schematic for the fluorescence polarization assay. When the miniprotein binds CCL25_AZ488, the size increases, as does the polarization of the emitted light. (C) The polarized fluorescent emission was measured for 15 nM CCL25_AZ488 in the presence of increasing concentrations of VUP binders. Binding of the miniproteins leads to an increase in polarization. Data points represent the average \pm SD of three independent experiments and internally normalized to the minimum and maximum polarization of each binder.

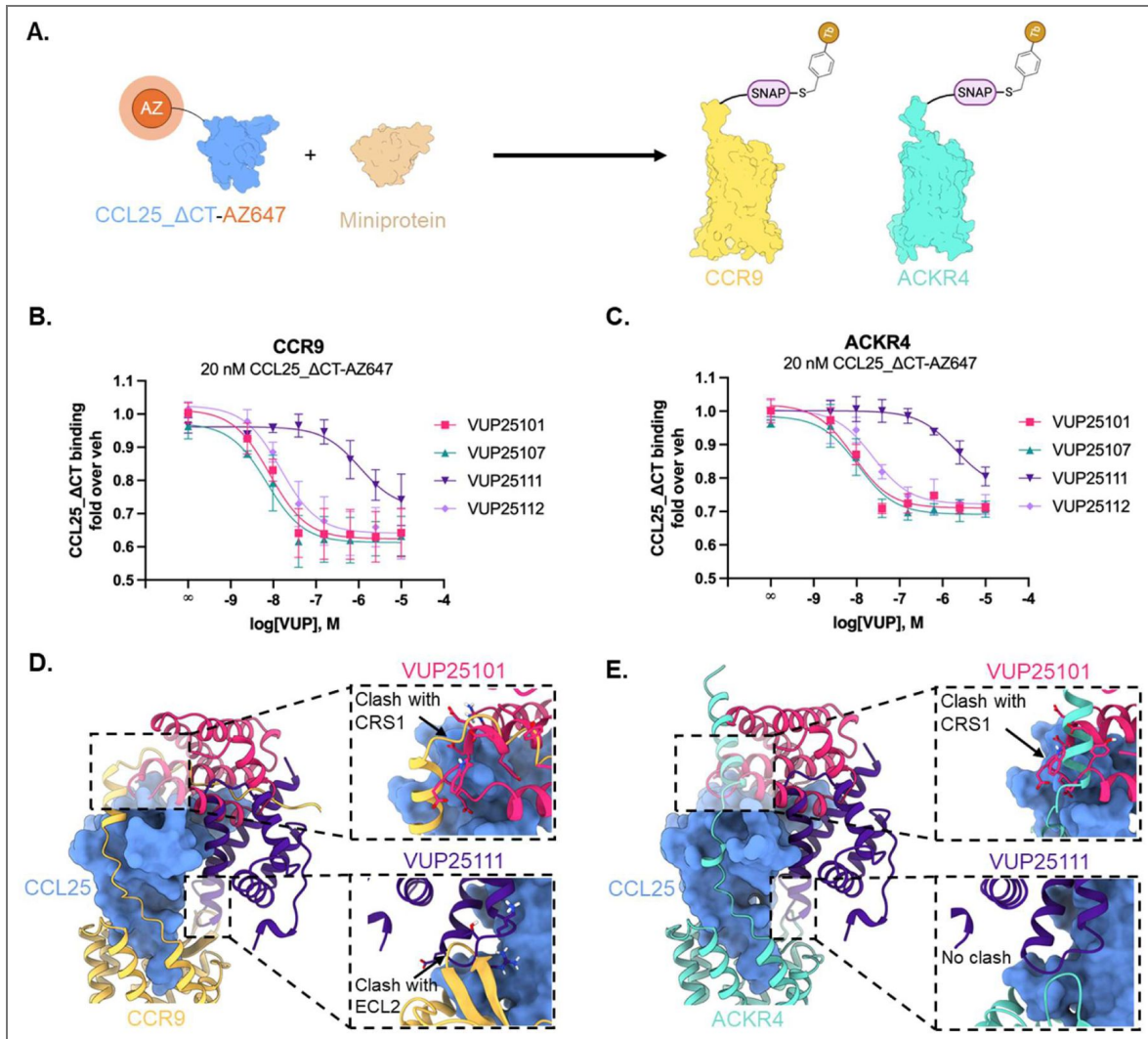


Figure 3. VUPs interfere with CCL25 binding to CCR9 and ACKR4 through clashes with CRS1.

(A) Design of binding assay using TR-FRET between CCL25_ΔCT-AZ647 and Terbium (Tb) labelled SNAP-CCR9 and SNAP-ACKR4. TR-FRET binding results for CCR9 (B) and ACKR4 (C) using 20 nM CCL25_ΔCT-AZ647 with increasing concentrations of the miniproteins, which shows a decreasing TR-FRET signal indicating an inability of the chemokine:VUP complex from binding the target receptor. Values represent the mean ± SD of three independent experiments performed in triplicate, presented as fold over vehicle condition. (D, E) Predicted structural models of VUP25101 and VUP25111 superimposed on the AF3-predicted CCR9:CCL25 (D) and ACKR4:CCL25 (E) complexes with zoom-in panels highlighting where the miniproteins are predicted to sterically clash with receptor:chemokine interactions.

confirmed by testing the miniproteins against arrestin recruitment to CXCR4 stimulated with CXCL12 (Fig. S5). No binder showed any effect on CXCL12-mediated CXCR4 activation at any concentration, thereby confirming that CCL25-mediated activation is specifically targeted.

CCL25-mediated arrestin recruitment to ACKR4 was also robustly inhibited by VUP25101 ($pIC_{50} = 7.73 \pm 0.74$) and VUP25107 ($pIC_{50} = 7.71 \pm 0.43$) (Fig. 4C [↗](#)). VUP25112 also completely impaired CCL25-mediated activation of the atypical receptor at the highest concentrations, but with significantly less potency ($pIC_{50} = 6.95 \pm 0.34$) compared to VUP25101 and VUP25107. The unique binder VUP25111, on the other hand, did not inhibit the activation of ACKR4 by CCL25 at any tested concentration. The lack of effect supports the structural interpretation that the CCL25:VUP25111 complex can bind ACKR4 as a cooperative unit and implies that this complex also does not alter the receptor's native, chemokine-promoted activation. These data indicate that CCL25-activation of both CCR9 and ACKR4 can be efficiently inhibited by targeting the CRS1-binding interface and suggest sufficient differences in the CCL25:receptor interface that allow receptor-specific inhibition.

G protein activation by CCR9 is inhibited by VUP25101, VUP25107, and VUP25112, but not VUP25111

Immune cell migration is driven in part by G protein coupling, thus, inhibition of this function is critical for crafting immune responses. The ability of the *de novo* binders to impact canonical G protein coupling was tested first by measuring the recruitment of 'mini' G proteins (mG_i), engineered Ras domain from $G\alpha_s$ with the interacting residues of G_i [42], to CCR9 by BRET between CCR9 C-terminally tagged with RlucII and mG_i fused to a Venus fluorophore (Fig. 5A [↗](#)). Like with arrestin recruitment, VUP25101 and VUP25107 showed identical inhibitory effects (VUP25101: $pIC_{50} = 8.17 \pm 0.21$; VUP25107: $pIC_{50} = 8.44 \pm 0.17$) on CCL25 promoted mG_i recruitment (Fig. 5B [↗](#)). Despite potent inhibition of arrestin engagement, VUP25112 showed a right-shifted IC_{50} value compared to the other binders ($pIC_{50} = 7.15 \pm 0.51$). Interestingly, VUP25111 showed no effect on the mG_i recruitment even at concentrations that robustly inhibited arrestin engagement. The deviations between the arrestin results (Fig. 4 [↗](#)) and G protein (Fig. 5B [↗](#)) suggest that the specific ligand interactions driving arrestin engagement with CCR9 may be more strict than for the G proteins.

GPCR signaling is amplified by a cascade and altered recruitment of the G protein effector may not be reflected in downstream outputs. CCR9 is G_i -coupled, and upon activation, the production of cAMP by the cell is inhibited, and the total concentration is lowered. The impact of the miniproteins on G protein signaling by CCR9 was monitored using a BRET-based cAMP biosensor (CAMYEL) to detect the inhibition of forskolin (FSK)-induced cAMP production (Fig. 5C [↗](#)). Downstream signaling was inhibited similar to mG_i recruitment, confirming the CCL25-targeting proteins are effective neutralizers of the chemokine-mediated signal (Fig. 5D [↗](#)). Like with mG_i , VUP25111 did not impact cAMP inhibition at any concentration, further confirming that the binder is not affecting G protein activation. Taken together with the complete suppression of arrestin recruitment, it appears that the binding of VUP25111 converts the balanced natural agonist CCL25 to G protein-biased towards CCR9.

VUP25111:CCL25 only partially impairs GPCR kinase 3 translocation to CCR9

The preserved G protein response from CCR9 (Fig. 5 [↗](#)) when treated with the VUP25111:CCL25 complex suggests greater complexity to how the miniprotein suppresses arrestin interactions. Arrestins are recruited to activated CCR9, like other GPCRs, following phosphorylation of the receptor C-terminus by GPCR kinases (GRKs) [41]. Thus, translocation readouts as seen in Fig. 4 [↗](#) report the combination of arrestin engagement and GRK phosphorylation and alterations to either event impact the response. To resolve if VUP25111 impairs the CCL25-mediated arrestin response through GRK phosphorylation, we measured the impact of the miniprotein binders on GRK3 recruitment to CCR9 by BRET between a nanoluciferase (Nluc) on GRK3 and a fluorophore (mV) on

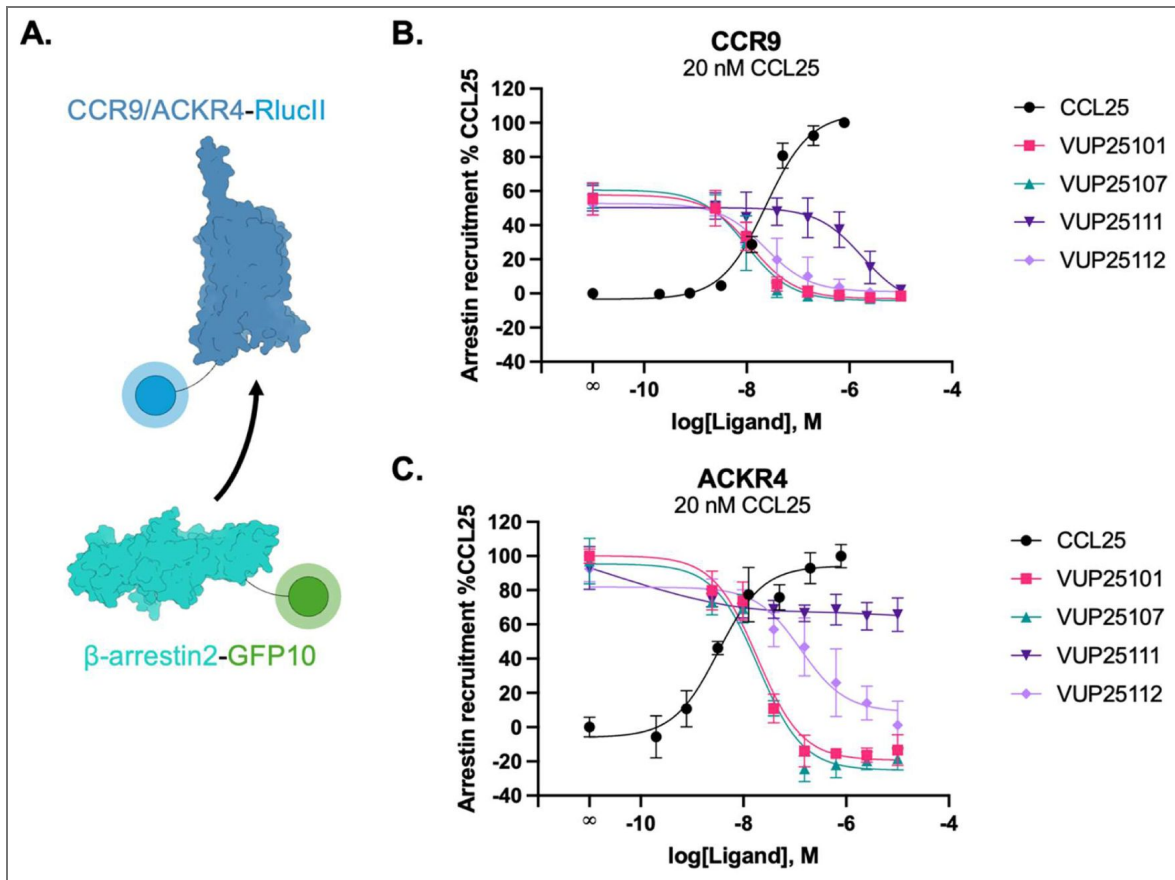


Figure 4. VUPs selectively inhibit CCL25-induced arrestin recruitment towards CCR9 and ACKR4.

(A) Schematic illustration of BRET sensor pair CCR9/ACKR4-RlucII and GFP10- β -arrestin2. The structure of β -arrestin2 is generated using AF3. β -Arrestin2 recruitment towards CCR9 (B) or ACKR4 (C) following stimulation across a titration of CCL25 concentrations (black) or a fixed concentration of CCL25 (20 nM) preincubated with increasing concentration of miniprotein. Values represent the mean \pm SD of three independent experiments performed in duplicate and normalized to min and max CCL25 response.

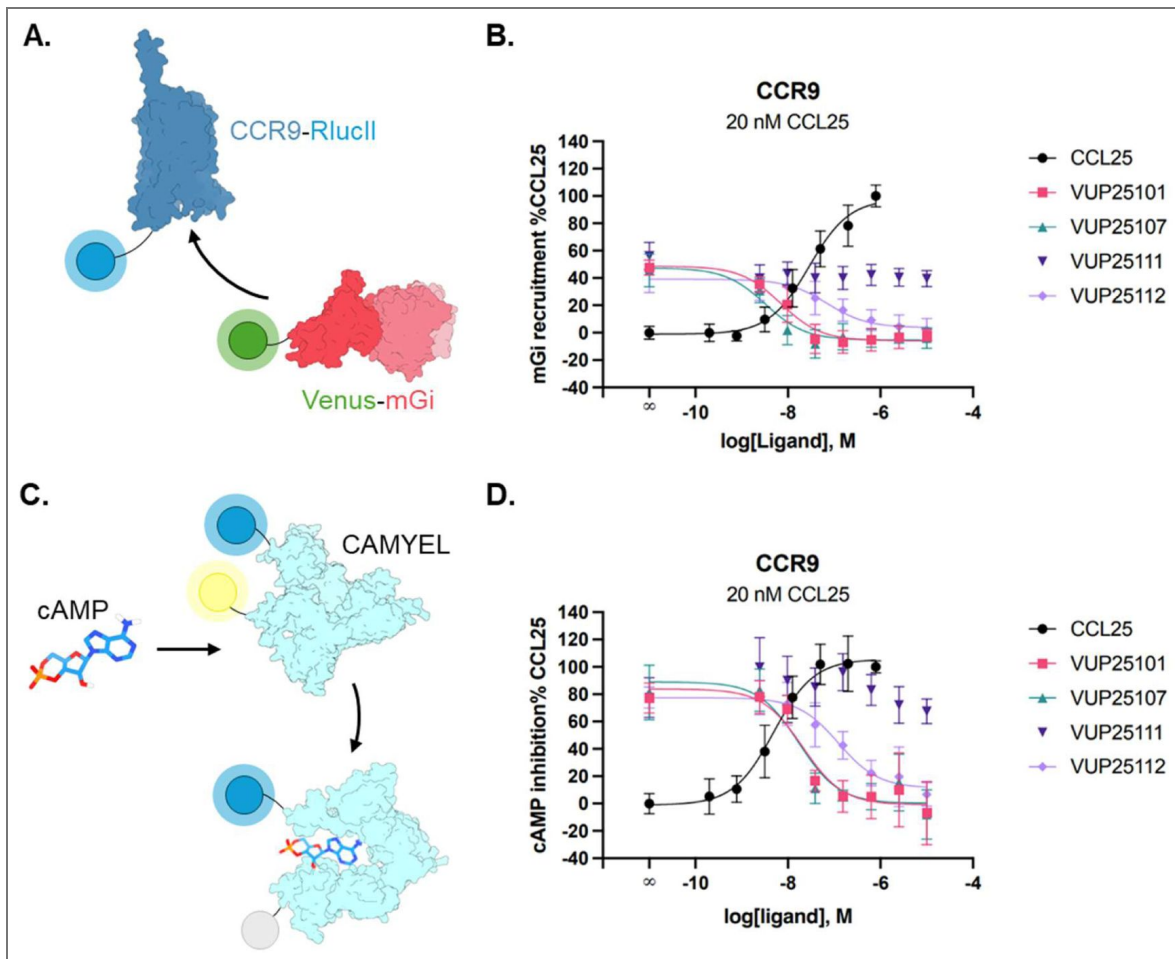


Figure 5. Most VUPs, but not VUP25111, effectively inhibit CCL25-induced G_i protein activation.

(A) Schematic illustration of BRET pair sensor CCR9 and Venus-mGi. The complex representing mGi is taken from PDB 9KO4[45]. (B) Concentration-dependent mGi recruitment to CCR9 following stimulation with a titration of CCL25 (black) or with 20 nM CCL25 preincubated with increasing concentrations of mini-proteins. (C) Suppression of cAMP signaling monitored by the BRET-based cAMP sensor CAMYEL. The structure of CAMYEL is generated using AF3. (D) CCR9 induced cAMP suppression following stimulation with a titration of CCL25 (black) or a fixed concentration of CCL25 (20 nM) preincubated with a titration of mini-proteins. Values represent mean \pm SD of three independent experiments performed in duplicate, normalized to min and max CCL25 response.

the receptor C-terminus (Fig. 6A [↗](#)). We have previously shown that, while all GRKs contribute of CCR9 phosphorylation, GRK3 shows the largest change in BRET upon recruitment to CCR9 [\[41\]](#). Similar to G protein and arrestin, the miniproteins which interfere with CRS1 interactions, VUP25101, VUP25107, and VUP25112, also prevent chemokine-induced relocation of GRK3 to CCR9 with similar inhibitory potency as arrestin and G proteins (VUP25101: $pIC_{50} = 8.40 \pm 0.04$; VUP25107: $pIC_{50} = 8.32 \pm 0.10$; VUP25112: $pIC_{50} = 7.81 \pm 0.46$) (Fig. 6B [↗](#)). Unexpectedly, VUP25111 treatment only partially inhibited GRK3 recruitment, but not the complete inhibition observed for these concentrations with arrestin recruitment. This suggests that the GRK interaction, and likely phosphorylation, is preserved with the VUP25111:CCL25 complex and arrestin engagement is not inhibited due to a lack of GRK phosphorylation.

Targeting CCL25 with miniproteins inhibit CCR9 internalization

GRK phosphorylation largely drives CCR9 internalization through coordinating arrestins as well as a not fully-described phosphorylation dependent mechanism [\[41\]](#). CCR9 internalization was tracked by BRET between CCR9-RlucII and a fluorophore (rGFP) anchored at the plasma membrane via a CAAX domain (rGFP-CAAX) (Fig. 7A [↗](#)) [\[43\]](#). Receptor trafficking away from the surface is then reported as a decrease in the BRET. Binding of VUP25101, VUP25107, or VUP25112 with CCL25 potently prevented the chemokine-mediated endocytosis of CCR9 (VUP25101: $pIC_{50} = 8.30 \pm 0.12$; VUP25107: $pIC_{50} = 8.35 \pm 0.16$; VUP25112: $pIC_{50} = 8.04 \pm 0.33$) (Fig 7B [↗](#)). Internalization was also blocked fully by VUP25111, albeit at substantially lower inhibitory potency ($pIC_{50} = 5.09 \pm 0.27$). These results suggest that the VUP25111:CCL25 complex suppresses both the arrestin dependent and independent internalization mechanisms used by CCR9, despite likely allowing for GRK phosphorylation.

Immune cell migration is inhibited by targeting CCL25 at the CRS1 interface

The goal of targeting CCL25 is to shape the CCR9-driven immune response to address inflammatory diseases of the bowels and inhibit CCR9-mediated metastasis of cancer cells. Migration of MOLT-4 cells, T lymphoblasts with native CCR9 expression (lacking significant ACKR4 expression [\[44\]](#)), was detected in a transwell format and quantified by counting the cells in the lower chamber with flow cytometry. The CCL25 concentration corresponding to the peak migratory signal (Fig. 8A [↗](#)) was added to the lower chamber with binder and total migrated cells were counted after 2 hours. Like with the G protein assays in Fig. 5 [↗](#), VUP25101 and VUP25107 severely impaired the CCL25-mediated migration of CCR9-expressing immune cells (Fig. 8B [↗](#)). VUP25112 was less effective at inhibiting migration, as half of the migratory response towards CCL25 was still present, reflecting a similar relative level of inhibition as observed for G protein coupling. MOLT-4 cell migration was unaffected by the inclusion of VUP25111, consistent with the apparent G protein bias imparted by this binder to CCL25. These results demonstrate conclusively the effectiveness of miniproteins targeting the CRS1 interaction between CCR9 and CCL25. Such targeting impairs immune cell motility and has the potential to modify immune responses.

Discussion

Figure 6. CCL25-mediated GRK3 recruitment to CCR9 is suppressed by VUP25101, VUP25107, and VUP25112, but not VUP25111.

(A) Schematic presentation of the GRK3 recruitment BRET setup to detect GRK3-Nluc translocation to activated CCR9-mV. (B) Recruitment of GRK3 to CCR9 measured by BRET across a concentration range of either CCL25 (black) or VUP mini-proteins with a constant 20 nM CCL25. Values represent mean \pm SD of three independent experiments performed in duplicate, normalized to min and max CCL25 response.

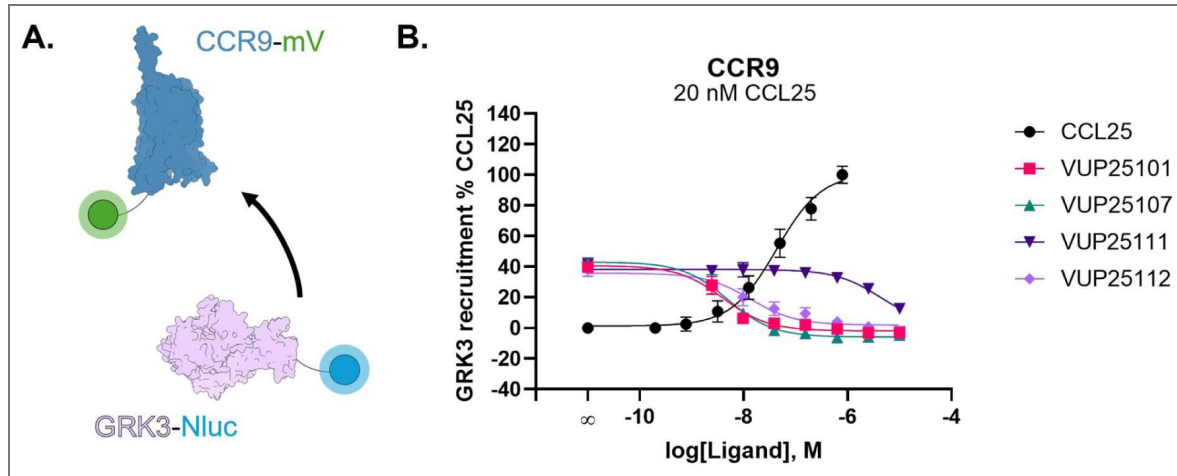
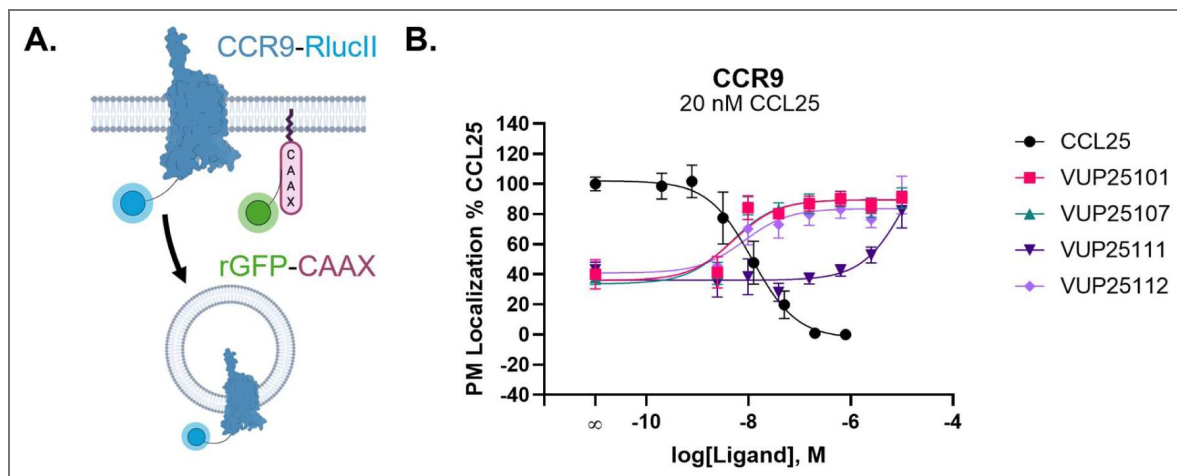


Figure 7. All VUPs inhibit CCL25-promoted internalization of CCR9.

(A) Schematic representation of the BRET assay to track CCR9 internalization by monitoring the resonance energy transfer between CCR9-RlucII and rGFP-CAAX. The BRET between the probes decreases as the receptor trafficks away from the membrane through internalization. (B) Internalization response measured by the BRET setup presented in (A) across a range of concentrations of CCL25 (black) or VUP mini-proteins with 20 nM CCL25. Values represent the mean \pm SD of three independent experiments performed in duplicate, normalized to min and max CCL25 response.



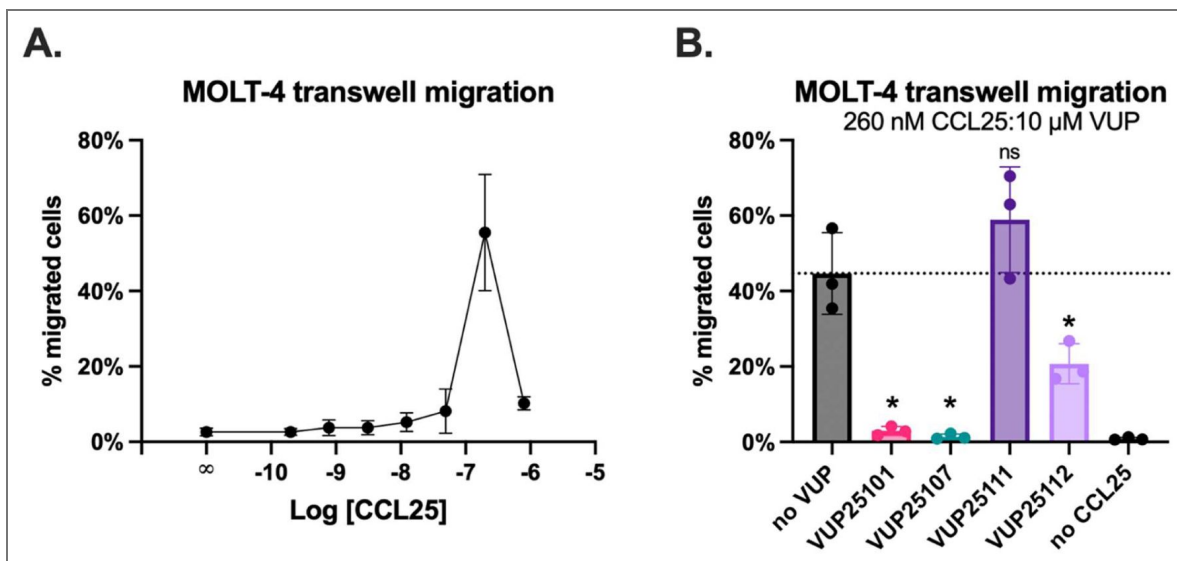


Figure 8. MOLT-4 chemotactic response towards CCL25 is suppressed by VUP binding.

(A) Percentage of migrated cells towards CCL25 across a titration of chemokine concentrations. (B) Percentage of migrated cells towards a fixed concentration of CCL25 (260 nM, corresponding to the highest migration observed in (A)) preincubated with miniproteins (10 μM). Values represent the mean ± SD of three independent experiments measured in technical triplicates by flow cytometry. Significance was determined using Welch ANOVA followed by a Dunnett's T3 multiple comparisons test comparing to no VUP. *p<0.05.

Dysregulation of the CCL25:CCR9 signaling axis has been implicated in promoting inflammatory diseases of the gut [17,18] and contributing to cancer metastasis [19,20]. Targeting this axis is a promising therapeutic approach and has produced many potential antagonists for CCR9 [46,47], but none have passed clinical trials [21]. Using advanced protein binder generation algorithms, miniproteins were designed to target CCL25 and prevent CCR9 activation by inhibition of agonist binding. Binders designed to block CRS1 interactions efficiently suppressed receptor activation and immune cell migration. Unexpectedly, targeting CCL25 along the chemokine β 1 strand, in the case of VUP25111, resulted in a miniprotein that inhibited CCR9-induced arrestin recruitment, but not G protein activation, as well as showing no inhibition of ACKR4. Thus, targeting CCL25 produced not only potent inhibitors, but also present new insights into signaling along the receptor:chemokine axis (Fig. 9 [↗](#)).

Modern methods to predict protein structures have advanced to produce highly accurate models, not only for individual proteins but also for protein-protein complexes. These algorithms can also be used to hallucinate fully new protein designs with specific functions [48,49]. Chemokines have proven difficult to target with small molecules for therapeutic applications, making them an excellent application for the BindCraft methodology. The generated miniproteins form a large interacting surface with the chemokines, providing sufficient binding interactions to efficiently engage the small protein agonists with high specificity. The miniproteins are about the size of chemokines and thus effectively block many of the interactions required for chemokine receptor engagement and subsequent receptor activation.

Chemokines generally bind their receptors in a multi-step process. First, the agonist engages the transmembrane bundle (CRS2). This interaction is subsequently stabilized by the receptor's N-terminus that wraps around the chemokine. Loss of the N-terminal interactions (CRS1) via receptor truncation drastically increases the rate of dissociation [9] and results in severely impaired receptor signaling [10]. Our unbiased approach to generating binders against CCL25 produced three miniproteins predicted to target the CRS1 interface and thus would only conflict with this secondary receptor N-terminal stabilizing interaction. Therefore, the robust inhibition observed with VUP25101, VUP25107, and VUP25112 suggests that blocking CRS1 contacts alone is sufficient to efficiently suppress chemokine-mediated activation of CCR9 and ACKR4, and that targeting interactions with the receptor or the orthosteric binding pocket is unnecessary for this effect. This also suggests that targeting other interacting interfaces, such as those involved in GAG binding or chemokine oligomerization, could have the added benefit of inhibiting receptor activation.

Our results show that the chemokine-targeting miniproteins displayed differential inhibition of the receptors. VUP25111 selectively suppressed CCL25-mediated arrestin recruitment to CCR9, but not ACKR4. An *in silico* structural analysis suggests that when complexed with CCL25, VUP25111 would clash with the modeled ECL2 of CCR9, thereby preventing proper binding of the chemokine. The same loop in ACKR4 is three residues shorter and can readily accommodate the larger complex. Binding and G protein activation results suggest that VUP25111 does not prevent CCL25 from binding CCR9, but instead modifies the agonist interactions to become G protein-biased, as discussed further below. Selectively inhibiting the canonical receptor without impairing its atypical partner would be advantageous when targeting chemokines. Suppressing the canonical migratory signals gives the desired modulation of the immune response. If binding to atypical scavenging receptors were also to be blocked, serum chemokine levels would increase in the absence this regulatory mechanism. The elevated chemokine concentrations could then dysregulate the signaling axis, mimicking an overexpression disease state. Such a condition may eventually overwhelm the inhibitors. Thus, continual removal of the agonist through native scavenging may be a necessary consideration when designing chemokine-targeting therapeutics.

Biased signaling with regard to GPCRs generally refers to preferential coupling to either G proteins or arrestins and can arise from specific ligands, receptor activation mechanisms, or cellular environment. VUP25111 prevents CCL25-induced arrestin recruitment to CCR9 but leaves G protein signaling intact. To our knowledge, this represents the first designed binder to alter the signaling bias of a natural ligand. Modeling the VUP25111:CCL25 complex with the predicted

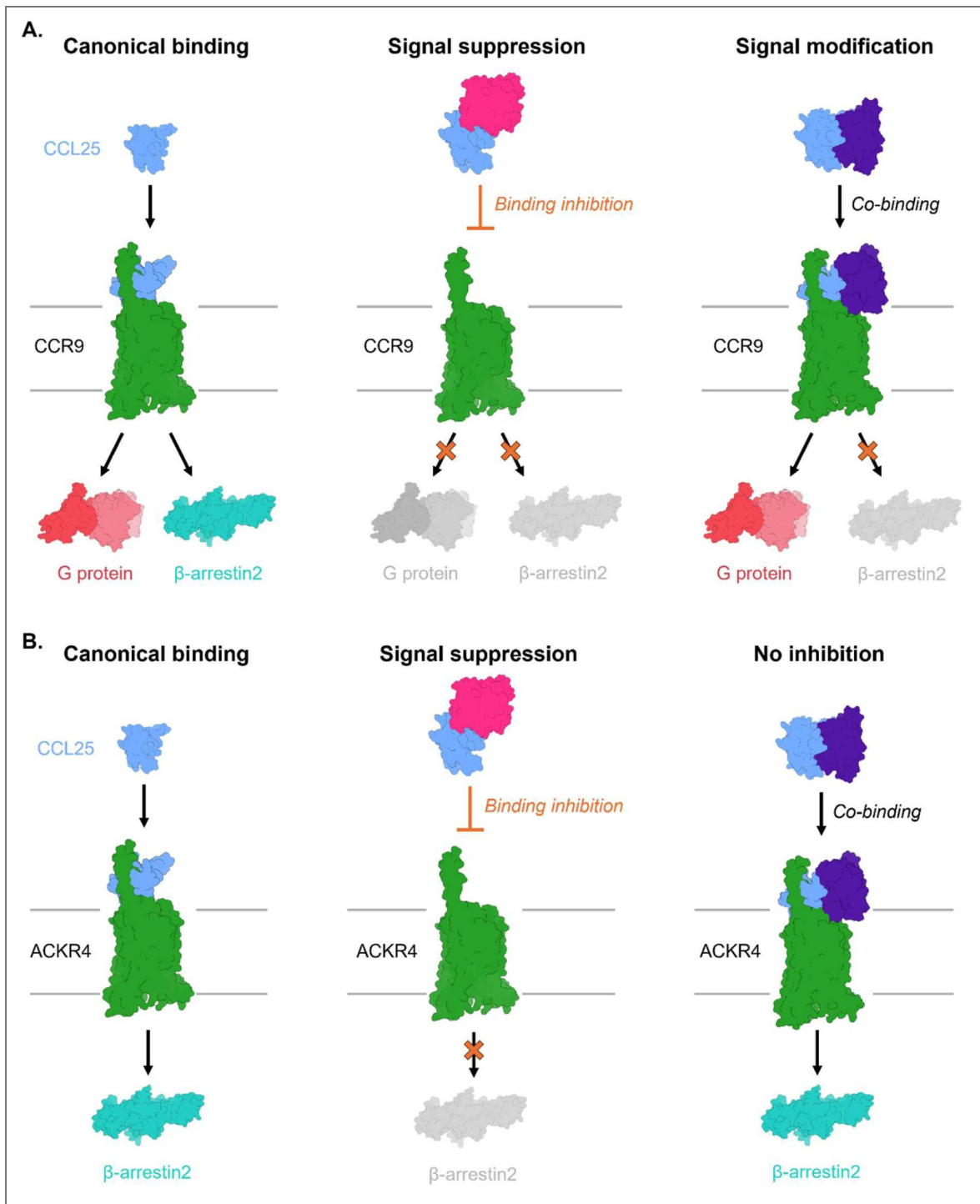


Figure 9. Mechanisms by which VUPs (VU mini-proteins) modulate CCL25 signaling at CCR9 and ACKR4.

(A) Canonical engagement of CCL25 with CCR9 produces a balanced signaling response, activating both G protein- and β -arrestin2-dependent pathways. Signal suppression occurs when mini-proteins (VUP25101, VUP25107, and VUP25112) sterically block CCL25:CCR9 interactions, leading to reduced activation of both G protein and β -m arrestin2 signaling. Signal modification can also arise from co-binding of the CCL25:mini-proteins complex to the receptor (VUP25111), resulting in biased signaling characterized by selective attenuation of the β -arrestin2 pathway while preserving G protein-mediated signaling for CCR9. (B) Canonical engagement of CCL25 with ACKR4 results in β -arrestin2 signaling. Signal suppression occurs when mini-proteins (VUP25101, VUP25107, and VUP25112) sterically block CCL25:ACKR4 interactions, leading to reduced β -arrestin2 signaling. Mini-protein VUP25111 does not inhibit activation of ACKR4 by CCL25. The complex representing G protein is taken from PDB 9KO4 [45], the structure of β -arrestin2 was generated using AF3.

binding position of CCL25 on CCR9 would cause a clash between the binder and ECL2 of the receptor. The fact that the same relative composition of binder to chemokine impairs arrestin coupling, but not G protein or GRKs, indicates that the VUP25111:CCL25 complex is able to bind and activate CCR9. While GRK recruitment is partially suppressed, the lack of complete inhibition likely indicates that the kinases can phosphorylate the VUP25111:CCL25 activated receptor. Thus, the complete inhibition of arrestin engagement cannot be easily explained by phosphorylation, and instead suggests the miniprotein:chemokine complex induces a conformational state incompatible with arrestins. Due to the clash with ECL2, the loop would need to distort to accommodate the larger ligand complex and this displacement may translate into the G protein and GRK permissive structural state. A similar signaling profile with intact G protein but no arrestin coupling was recently observed by a CCR9 point mutation (T208^{5,32}A) immediately following ECL2 [50], however, we were unable to replicate these dramatic results (Fig. S6). Instead, the smaller residue showed exactly WT-like effector coupling in our experiments. The β 1-binding interface of VUP25111 is similar to how CXC chemokine ligands, like CXCL12, dimerize. When the CXCL12 dimer binds its canonical receptor CXCR4, the second chemokine would also cause a large deflection of ECL2 of the receptor. Signaling of dimeric CXCL12 through CXCR4 is also biased completely towards G proteins, analogous to the effects of VUP25111 on CCL25 activation of CCR9 [51]. While G protein signaling was largely intact with dimeric CXCL12 activation of CXCR4, migration was eliminated, unlike what is shown here for CCR9. This suggests that different mechanisms of migration are likely present for the different receptors and different cell lines, and CCR9-mediated migration of MOLT-4 cells is exclusively dependent on G protein activation.

Targeting the chemokines of the chemokine receptor system has proven to be an evolutionarily efficient method to modulate immune responses. Atypical chemokine receptors scavenge chemokines to direct canonical receptor-mediated migration. Ticks and viruses target these agonists to suppress immune responses during blood meals and infection, respectively. Here, this mechanism is exploited through *de novo* binder design, demonstrating the potential application of new AI methods to generate novel binders with new modalities. The miniproteins are valuable research tools to study chemokines and the receptor:chemokine signaling pathways and offer new options for drug discovery programs. These results provide a framework for therapeutically targeting difficult-to-modulate chemokine receptors and reveal unexpected mechanisms for signaling bias.

Materials and Methods

Unless otherwise stated, all materials and reagents were purchased from Melford or Sigma-Aldrich. Prolume purple was purchased from Nanolight Technologies (Prolume Ltd.). All miniprotein expression plasmids were synthesized by and purchased from Genscript. Full length CCL25-AZ488 and CCL25_ΔCT-AZ647 (1-77) were purchased from Protein Foundry.

Generation of *de novo* binders

The three-dimensional structure of human CCL25 was retrieved from the AlphaFold Protein Structure Database [37]. To produce the mature form of the chemokine, the N-terminal signal sequence (M1-T23) was removed and residue numbering was reset to begin with Q1. Additionally, the C-terminus was truncated to L77 to focus the binders to the chemokine fold and yield a model of CCL25_ΔCT (1-77). Binder designs were generated with BindCraft [31] (version 1.5.0) using default_filters and the default_4stage_multimer protocol. Binders were allowed to have a length of between 75 and 125 amino acids. No hotspot residues were specified, thereby allowing the design algorithm to explore binding across the entire accessible surface of CCL25. In total, 101 designs were generated that passed computational filters and ranked using the ipTM score.

Comparison of structural similarity among binders was performed using the calculation of TM-scores using TM-align [52]. For each complex, the binder chain was extracted, and all pairwise combinations of generated binders were aligned using TM-align. To obtain a low-dimensional

representation of structural relationships, TM-scores were converted to a distance matrix (1 – TM-score), and a two-dimensional embedding was generated using UMAP [53] (n_neighbors = 10, min_dist = 0.1, metric = “precomputed”).

Molecular interactions between the miniproteins designs and CCL25 were calculated with ProLIF [54] using the outputted structure from BindCraft.

Molecular dynamics simulations

Complexes from BindCraft were prepared using the CHARMM-GUI [55] solution builder. Protonation states of residues were assigned at pH 7.4 within the CHARMM-GUI solution builder. For terminal group patching, the N-terminus was acetylated (ACE patch), and the C-terminus was methylamidated (CT3 patch). The complexes were solvated in a cubic water box with a 10 Å buffer and neutralized to 0.15 M NaCl. The CHARMM36m force-field [56] parameters were used for the proteins and ions, while the TIP3P model was used for water.

All MD simulations were performed using GROMACS 2025.1 [57]. Systems were first minimized using a 5000-step steepest-descent minimization (≤ 5000 steps; convergence threshold 1000 kJ/mol/nm). Subsequently, the system was equilibrated according to the protocol generated by CHARMM-GUI. Systems were subjected to a 125-ps NVT run with a 1 fs time step and positional restraints on all protein heavy atoms (force constants: 400 kJ/mol/nm² for backbone atoms and 40 kJ/mol/nm² for side chains). Initial velocities were generated from a Maxwell-Boltzmann distribution at 310.15 K. Temperature was maintained at 310.15 K using the v-rescale thermostat [58]. Production simulations were run for 100 ns in the NPT ensemble. The v-rescale thermostat was used to maintain a temperature of 310.15 K, and the pressure was kept at 1 bar via semi-isotropic coupling to the c-rescale barostat [59] ($\tau_p = 5.0$ ps, compressibility = 4.5×10^{-5} bar). Bond lengths of hydrogen covalent bonds were constrained using the LINCS algorithm. Long-range electrostatic interactions were calculated with the particle mesh Ewald method and the Verlet cutoff scheme with a 1.2 nm cutoff for both PME electrostatics and Lennard-Jones interactions, the latter using a force-switch modifier between 1.0 and 1.2 nm. Atomic positions were saved every 50 ps.

Trajectory analysis was performed using GROMACS and MDAnalysis [60]. For each system, backbone RMSD, binding-site RMSD, and all-atom RMSD were calculated. These were done with proper masking in MDAnalysis. Binding free energies were estimated using gmx_MMPBSA [61] with the MM-GBSA method (igb = 5, 0.15 M salt). For each trajectory, 1001 frames (sampled every 100 ps over a 100 ns simulation) were included.

AlphaFold3 structure prediction

The AlphaFold3 [62] server was used to predict the structures of CCL25 (CCL25-CT, 1-77) bound to CCR9 and ACKR4. Sequences of CCL25 (UniProt: O15444), CCR9 (UniProt: P51686), and ACKR4 (UniProt: Q9NPB9) were retrieved from UniProt [63]. For each complex, five models were generated using default settings, and the top-ranked model was selected for visualization.

DNA Constructs and site-directed mutagenesis

Human CCR9 (1-369) and ACKR4 (1-350) were cloned into a pcDNA3.1 expression vector either alone or followed by a C-terminal RLucII tag as described previously [41]. For receptor binding assays, hCCR9 and hACKR4 were cloned into a pcDNA5 expression vector, wherein the mammalian promoter was replaced with EF1a promoter, preceded by a N-terminal SNAP-tag. GFP10- β -arrestin2 (gifted from N. Heveker, Université de Montréal) [64], NES-Venus-mGs/i143 (mG_i) [42], and mCitrine-EPAC-Rluc (CAMYEL) [65,66] were described previously. Site-directed mutagenesis was performed using the Q5 mutation kit (NEB) and confirmed by sanger sequencing.

Chemokine purification from *E. Coli*

The chemokines CCL25 and CXCL12 were expressed and purified in *E.coli* following previously established protocols [41,67]. Briefly, codon optimized chemokine sequences containing the 8x histidine-tag and enterokinase cleavage site were cloned into a pET21 vector. The synthesized plasmid was transformed into *E.coli* BL21(DE3)pLysS cells and protein expression was triggered by Isopropyl- β -D-thiogalactopyranoside (IPTG) induction. Inclusion bodies containing the chemokines were harvested by sonication and solubilized in a buffer composed of 50 mM Tris, 6 M guanidine-HCl, and 300 mM NaCl at pH 8.0. Next, the solubilized protein was purified using a nickel-nitrotriacetic acid (Ni-NTA) affinity column, subsequently washed with 50 mM MES, 6 M guanidine-HCl, 300 mM NaCl pH 6.0 and eluted with 50 mM acetate, 6 M guanidine-HCl, 300 mM NaCl pH 4.0. The elution fraction was refolded in 50 mM Tris, 700 mM arginine-HCl, 1 mM EDTA, 1 mM GSSG, 200 mM glutamine, 0.1% Triton-X pH 7.5 by dropwise addition. After refolding, the protein was dialyzed in 20 mM Tris with 150 mM NaCl pH 8.0. The 8xHis-tag was removed using Enterokinase (New England Biolabs), and cleavage was confirmed by SDS-PAGE and LC-MS. The tag-free chemokine was further purified on a Ni-NTA column, washing with 50 mM Tris pH 8.0, and elution in 6 M guanidine-HCl using either 50 mM MES (pH 6.0) or 50 mM acetate (pH 4.0) in two separate fractions. Next, these fractions were purified by reverse-phase HPLC on a Gemini C18 110A column (Phenomenex) with a linear 5-95% acetonitrile gradient in 0.1% TFA. The final purified chemokines were validated by LC-MS, lyophilized, and stored at -80 °C.

VUP purification from *E. Coli*

Plasmids encoding VUP constructs, N-terminally preceded by a 6x histidine purification tag, were transformed into *E. coli* BL21(DE3)pLysS by standard heat-shock transformation and plated on LB agar containing kanamycin (100 ug/mL). A single colony of each construct was inoculated into 5-10 mL LB supplemented with kanamycin (100 ug/mL) and grown overnight at 37 °C while shaking (300 rpm) to generate starter culture. The following day, 1:25 dilutions of overnight culture were made into fresh LB containing kanamycin (100 ug/mL) and grown at 37 °C while shaking (300 rpm) until mid-log phase (OD600 ~ 0.6-0.8). Protein expression was induced by addition of IPTG to a final concentration of 1 mM, followed by incubation of cultures for 5-6 hour at 37 °C while shaking. Cell pellets were resuspended in TBS (50 mM Tris pH 7.4, 150 mM NaCl) supplemented with DNaseI (Thermo Fisher) and protease inhibitors (cOmplete, EDTA-free) and subsequently lysed by sonication. Centrifugation was repeated under the same conditions as described earlier. Imidazole was added to the supernatant for final concentration of 20 mM. Prior to applying the supernatant, Ni-NTA columns were equilibrated in TBS with 20 mM imidazole. The columns were washed with 5 column volumes of TBS containing 20 mM imidazole to remove non-specifically bound proteins. Lastly, VUPs were eluted with TBS containing 300 mM imidazole. All fractions were analyzed by SDS-PAGE to assess the purity of the protein. Eluted VUP fractions were concentrated using a 15 kDa spin filter and buffer-exchanged with 4 column volumes of TBS and stored at -80 °C. The isoelectric point of VUP25111 is near physiological pH, thus the protein was buffer exchanged to 50 mM MES pH 6.0 150 mM NaCl to improve solubility and stability for long term storage.

Chemokine-miniprotein complex formation by fluorescence polarization

Fluorescently tagged CCL25 (CCL25-AZ488; final concentration 15 nM) was mixed 1:1 with VUP binders prepared in TRIS buffer (50 mM, pH 7.7) supplemented with 0.05% Pluronic Acid and dispensed into a black 384-well microplate (Greiner, F-bottom). VUP binder solutions began at 10 μ M and were tested in a fourfold serial dilution series. Fluorescence polarization measurements were performed using a PHERAstar plate reader set at 25 °C. The fluorescently labeled chemokine CCL25-AZ488 was excited at 485 nm, and emission was detected at 520 nm. The target milli polarization (mP) value was set to 20 and calibrated using the positive control (CCL25-AZ488 (15 nM) in buffer alone). Polarization data was calculated according to the standard equation:

$$mP = 1000x \frac{I_{\parallel} - G \cdot I_{\perp}}{I_{\parallel} + G \cdot I_{\perp}}$$

Where I_{\parallel} and I_{\perp} represent the fluorescence intensities measured parallel and perpendicular to the plane of polarized excitation light, respectively. The results of three independent assays were normalized to vehicle and highest response, as displayed.

Transfection of HEK293 Cells

HEK293T cells (ATCC) were cultured in Dulbecco's Modified Eagle's Medium (DMEM, Thermo Fisher Scientific) containing 1% penicillin + streptomycin (Gibco), and 10% Fetal Bovine Serum (FBS, Bodinco) kept at 37 °C with 5% CO₂ in a humidified environment. Cells were transfected with 2 µg DNA per 1 million cells using 6 µg polyethyleneimine (PEI, Polysciences Inc.) in 150 mM NaCl. The DNA-PEI mixtures were incubated for 15 minutes at room temperature (RT). Cells were detached using trypsin/EDTA solution (Thermo Fisher Scientific) and resuspended in DMEM. Cells were counted and then added to the DNA-PEI mixture. Cells were seeded at 30k/well on a white 96-well plate (Greiner) and incubated for 48 hour before readout.

Inhibition of CCL25 binding to receptors by TR-FRET

To make SNAP-CCR9 or SNAP-ACKR4 membranes, HEK293T cells were transfected with 2 µg of SNAP-GPCR DNA per 2 million cells using OptiMEM (Gibco) and PEI as described above. After 48 hour, cells were harvested in PBS at 4 °C and subsequently centrifuged for 10 minutes at 1500 x g. Pelleted membranes were resuspended in NaPO₄ + 0.05% Pluronic acid and homogenized by sonication. Next, cells were centrifuged at 22000 x g and resuspended in NaPO₄ + 0.05% Pluronic acid and labelled with 100 nM Tag-lite SNAP-Lumi4-Tb labeling reagent (Revvity) for 1 hour at 37 °C. To wash of free label, membranes were washed at least five times with NaPO₄ + 0.05% Pluronic acid. Membranes were homogenized again by sonication, snap frozen in liquid nitrogen, and stored at -80 °C. CCL25_ΔCT-AZ647 (20 nM) was incubated for 30 min at RT with increasing concentrations of the miniproteins.

Next, the receptor suspension was homogenized by sonication before adding it to the readout plate (96 well half-area microplate, Greiner). The CCL25_ΔCT-AZ647+VUP mixture was added to the membranes and centrifuged at 150 x g for 3 min before incubation for 30 min at RT. TR-FRET ratio was quantified using a PHERAstar plate reader equipped with an optic module that excites at 337 nm and measures at 620 nm (Tb) and 665 nm (FRET signal) using 400 flashes per well. TR-FRET ratio was determined by dividing the FRET intensity by the Tb intensity using a ratio factor of 10000.

β-Arrestin2 recruitment by BRET

HEK293T cells were transfected with 50 ng receptor-RlucII and 1 µg GFP10-β-arrestin2 up to an amount of 2 µg with empty pcDNA3.1 as described previously [41]. After 48 hour incubation, cells were rinsed once with Phosphate Buffered Saline (PBS) and kept in Hank's balanced salt solution (HBSS) supplemented with 0.1% bovine serum albumin (BSA; Fraction V; PanReac Applichem). 5 µM of Prolume Purple (Prolume Ltd.) was added and incubated for 5-10 minutes at 37 °C. Cells were then stimulated with increasing concentrations of either CCL25 or VUP binders containing fixed CCL25 (20 nM). A PHERAstar plate reader (BMG) was used for 1 hour at 37 °C to measure bioluminescence at 410-80 nm and 515-30 nm. BRET values were determined as the ratio of red and blue luminescence (515-30/410-80). The results of three independent assays were normalized to the mock (no chemokine) and highest CCL25 concentration.

mG_i recruitment by BRET

HEK293T cells were transfected with 50 ng CCR9-RlucII and 250 ng Venus-mG_i up to an amount of 2 µg with pcDNA3.1 as described previously [41]. After 48 hour incubation, cells were rinsed once with PBS and kept in HBSS supplemented with 0.1% BSA. 5 µM of Coelenterazine-h (CTZ-h, Promega) was added to the cells and incubated for ~5 minutes at 37 °C. Cells were then stimulated with increasing concentrations of CCL25 or a fixed concentration of CCL25 (20 nM) pre-incubated

with increasing concentrations of the miniproteins for 30 min. A PHERAstar plate reader was used for 1 hour at 37 °C to measure bioluminescence at 475-30 nm and 535-30 nm. BRET values were determined as the ratio of red and blue luminescence (535-30/475-80). The results of three independent assays were normalized to the mock (no chemokine) and highest CCL25 concentration.

cAMP measurement by BRET

HEK293T cells were transfected with 400 ng untagged CCR9 and 800 ng CAMYEL (cAMP sensor using YFP-Epac-Rluc) up to an amount of 2 µg with pcDNA3.1 as described previously [41]. After 48 hour incubation, cells were rinsed once with PBS and kept in HBSS supplemented with 0.1% BSA. 5 µM of Coelenterazine-h (CTZ-h, Prolume Ltd) was added to the cells and incubated for ~5 minutes (37 °C) as described before (see; Mini-Gi recruitment by BRET). After, cAMP levels were amplified with 10 µM forskolin (FSK, Sigma-Aldrich), and the bioluminescence was measured for ~8 minutes. Cells were then stimulated with increasing concentrations of CCL25 or a fixed concentration of CCL25 (20 nM) pre-incubated with increasing concentrations of the miniproteins for 30 minutes. The results of three independent assays were normalized to the mock (no chemokine) and highest CCL25 concentration.

GRK3 recruitment by BRET

HEK293T cells were transfected with 250 ng CCR9-mV and 50 ng GRK3-nLuc up to an amount of 2 µg with empty pcDNA3.1 as described previously [41]. After 48 hour incubation, cells were rinsed once with PBS and kept in HBSS supplemented with 0.1% BSA. 20 µM of 400A (Bld. Pharma.) was added and incubated for 5-10 minutes at 37 °C. Cells were then stimulated with increasing concentrations of either CCL25 or VUP binders containing fixed CCL25 (20 nM). A PHERAstar plate reader (BMG) was used for 1 hour at 37 °C to measure bioluminescence at 475-30 nm and 535-30 nm. BRET values were determined as the ratio of red and blue luminescence (535-30/475-80). The results of three independent assays were normalized to the mock (no chemokine) and highest CCL25 concentration.

CCL25-mediated internalization by BRET

HEK293T cells were transfected with 50 ng CCR9-RlucII and 200 ng rGFP-CAAX up to an amount of 2 µg with empty pcDNA3.1 as described previously [41]. After 48 hour incubation, cells were rinsed once with PBS and kept in HBSS supplemented with 0.1% BSA. 5 µM of Prolume Purple (Prolume Ltd.) was added and incubated for 5-10 minutes at 37 °C. Cells were then stimulated with increasing concentrations of either CCL25 or VUP binders containing fixed CCL25 (20 nM). A PHERAstar plate reader (BMG) was used for 1 hour at 37 °C to measure bioluminescence at 410-80 nm and 515-30 nm. BRET values were determined as the ratio of red and blue luminescence (515-30/410-80). The results of three independent assays were normalized to the mock (no chemokine) and highest CCL25 concentration.

Molt-4 cell migration quantified by flow cytometry

Transwell chemotaxis assays were performed using TC inserts for 24-well plates, 8 µm pore size (Sarstedt). MOLT-4 cells (ATCC) were collected by centrifugation at 125 x g for 5 min and subsequently resuspended in RPMI 1640 + 10% FBS (Gibco) at a density of 400k/ml. Next, 80k cells were added to the inserts and placed in the 24-well plate with either an increasing concentration of CCL25 or a fixed concentration of CCL25 (260 nM) together with 10 µM of miniprotein in the bottom chamber (pre-incubated for 30 min). The plate was then incubated for 2 hour at 37°C in a humidified atmosphere with 5% CO₂. After incubation, cells in bottom chamber were counted using a Guava easyCyte flow cytometer (Cytex) as three technical replicates. Data is presented as percentage of migrated cells relative to the initial number of cells in the insert.

Data availability

All relevant data supporting this study are included in the article or source data files.

Additional information

Funding

This publication is part of the project TRANSLATION with file number OCENW.M.24.006 which is partly financed by the Dutch Research Council (NWO) under the grant [grant ID: <https://doi.org/10.61686/YKUZU08217>].

Funding

Funder	Grant reference number	Author
Nederlandse Organisatie voor Wetenschappelijk Onderzoek (NWO)	https://doi.org/10.61686/YKUZU08217 7	Christopher T Schafer

Author ORCID iDs

Bas de Boer: <https://orcid.org/0009-0004-2024-4704>
Thomas D Lamme: <https://orcid.org/0009-0005-2168-9809>
Csongor G Németh: <https://orcid.org/0009-0009-6422-3557>
Elisabeth M Elfrink: <https://orcid.org/0009-0003-2484-9666>
Martine J Smit: <https://orcid.org/0000-0003-2713-0238>
Iwan JP de Esch: <https://orcid.org/0000-0002-1969-0238>
Christopher T Schafer: <https://orcid.org/0000-0001-9907-295X>

Additional files

[Supplemental Information](#)

References

- [1] **Boldajipour B.**, Mahabaleshwar H., Kardash E., Reichman-Fried M., Blaser H., Minina S., Wilson D., Xu Q., Raz E. (2008) Control of Chemokine-Guided Cell Migration by Ligand Sequestration. *Cell* **132**:463-473 <https://doi.org/10.1016/J.CELL.2007.12.034> | PubMed
- [2] **Koelink P.J.**, Overbeek S.A., Braber S., De Kruijf P., Folkerts G., Smit M.J., Kraneveld A.D. (2012) Targeting chemokine receptors in chronic inflammatory diseases: An extensive review. *Pharmacol. Ther* **133**:1-18 <https://doi.org/10.1016/J.PHARMTHERA.2011.06.008> | PubMed
- [3] **Szekanecz Z.**, Koch A.E. (2015) Successes and failures of chemokine-pathway targeting in rheumatoid arthritis. *Nature Reviews Rheumatology* **12**:5-13 <https://doi.org/10.1038/nrrheum.2015.157> | PubMed
- [4] **O'Hayre M.**, Salanga C.L., Handel T.M., Hamel D.J. (2010) Emerging concepts and approaches for chemokine-receptor drug discovery. *Expert Opin. Drug Discov* **5**:1109-1122 <https://doi.org/10.1517/17460441.2010.525633> | PubMed
- [5] **Dyer D.P.** (2020) Understanding the mechanisms that facilitate specificity, not redundancy, of chemokine-mediated leukocyte recruitment. *Immunology* **160**:336-344 <https://doi.org/10.1111/imm.13200> | PubMed
- [6] **Kufareva I.**, Gustavsson M., Zheng Y., Stephens B.S., Handel T.M. (2017) What Do Structures Tell Us About Chemokine Receptor Function and Antagonism?. *Annu. Rev. Biophys* **46**:175-198 <https://doi.org/10.1146/annurev-biophys-051013-022942> | PubMed
- [7] **Sonawani A.**, Kharche S., Dasgupta D., Sengupta D. (2022) Insights into the dynamic interactions at chemokine-receptor interfaces and mechanistic models of chemokine binding. *J. Struct. Biol* **214** <https://doi.org/10.1016/J.JSB.2022.107877> | PubMed
- [8] **Kayastha K.**, Zhou Y., Brünle S. (2024) Structural perspectives on chemokine receptors. *Biochem. Soc. Trans* **52**:1011 <https://doi.org/10.1042/BST20230358> | PubMed

- [9] Gustavsson M., Dyer D.P., Zhao C., Handel T.M. (2019) Kinetics of CXCL12 binding to atypical chemokine receptor 3 reveal a role for the receptor N-terminus in chemokine binding. *Sci. Signal* **12** <https://doi.org/10.1126/SCISIGNAL.AAW3657> | PubMed
- [10] Stephens B.S., Ngo T., Kufareva I., Handel T.M. (2020) Functional anatomy of the full-length CXCR4-CXCL12 complex systematically dissected by quantitative model-guided mutagenesis. *Sci. Signal* **13** <https://doi.org/10.1126/scisignal.aay5024> | PubMed
- [11] Wescott M.P., Kufareva I., Paes C., Goodman J.R., Thaker Y., Puffer B.A., Berdougou E., Rucker J.B., Handel T.M., Doranz B.J. (2016) Signal transmission through the CXC chemokine receptor 4 (CXCR4) transmembrane helices. *Proc. Natl. Acad. Sci. U. S. A* **113**:9928-9933 <https://doi.org/10.1073/pnas.1601278113> | PubMed
- [12] Gustavsson M., Wang L., Van Gils N., Stephens B.S., Zhang P., Schall T.J., Yang S., Abagyan R., Chance M.R., Kufareva I., et al. (2017) Structural basis of ligand interaction with atypical chemokine receptor 3. *Nature Communications* **8**:8 <https://doi.org/10.1038/ncomms14135> | PubMed
- [13] Papadakis K.A., Prehn J., Nelson V., Cheng L., Binder S.W., Ponath P.D., Andrew D.P., Targan S.R. (2000) The Role of Thymus-Expressed Chemokine and Its Receptor CCR9 on Lymphocytes in the Regional Specialization of the Mucosal Immune System. *The Journal of Immunology* **165**:5069-5076 <https://doi.org/10.4049/JIMMUNOL.165.9.5069> | PubMed
- [14] Zaballos A., Gutiérrez J., Varona R., Ardavin C., Márquez G. (1999) Cutting Edge: Identification of the Orphan Chemokine Receptor GPR-9-6 as CCR9, the Receptor for the Chemokine TECK. *The Journal of Immunology* **162**:5671-5675 <https://doi.org/10.4049/JIMMUNOL.162.10.5671>
- [15] Wurbel M.A., Malissen B., Campbell J.J. (2006) Complex regulation of CCR9 at multiple discrete stages of T cell development. *Eur. J. Immunol* **36**:73-81 <https://doi.org/10.1002/EJL.200535203> | PubMed
- [16] Uehara S., Grinberg A., Farber J.M., Love P.E. (2002) A role for CCR9 in T lymphocyte development and migration. *J. Immunol* **168**:2811-2819 <https://doi.org/10.4049/JIMMUNOL.168.6.2811> | PubMed
- [17] Koenecke C., Förster R. (2009) CCR9 and inflammatory bowel disease. *Expert Opin. Ther. Targets* **13**:297-306 <https://doi.org/10.1517/14728220902762928> | PubMed
- [18] Wu X., Sun M., Yang Z., Lu C., Wang Q., Wang H., Deng C., Liu Y., Yang Y. (2021) The Roles of CCR9/CCL25 in Inflammation and Inflammation-Associated Diseases. *Front. Cell Dev. Biol* **9** <https://doi.org/10.3389/FCELL.2021.686548> | PubMed
- [19] Wendt E., Keshav S. (2015) CCR9 antagonism: potential in the treatment of Inflammatory Bowel Disease. *Clin. Exp. Gastroenterol* **8**:119 <https://doi.org/10.2147/CEG.S48305> | PubMed
- [20] Letsch A., Keilholz U., Schadendorf D., Assfalg G., Asemisen A.M., Thiel E., Scheibenbogen C. (2004) Functional CCR9 expression is associated with small intestinal metastasis. *J. Invest. Dermatol* **122**:685-690 <https://doi.org/10.1111/J.0022-202X.2004.22315.X> | PubMed
- [21] Feagan B.G., Sandborn W.J., D'Haens G., Lee S.D., Allez M., Fedorak R.N., Seidler U., Vermeire S., Lawrance I.C., Maroney A.C., et al. (2015) Randomised clinical trial: vécirnon, an oral CCR9 antagonist, vs. placebo as induction therapy in active Crohn's disease. *Aliment. Pharmacol. Ther* **42**:1170-1181 <https://doi.org/10.1111/APT.13398> | PubMed
- [22] Alcami A., Saraiva M. (2009) Chemokine Binding Proteins Encoded by Pathogens. *Adv. Exp. Med. Biol* **666**:167-179 https://doi.org/10.1007/978-1-4419-1601-3_13 | PubMed
- [23] Bhusal R.P., Eaton J.R.O., Chowdhury S.T., Power C.A., Proudfoot A.E.I., Stone M.J., Bhattacharya S. (2020) Evasins: Tick Salivary Proteins that Inhibit Mammalian Chemokines. *Trends Biochem. Sci* **45**:108-122 <https://doi.org/10.1016/J.TIBS.2019.10.003> | PubMed
- [24] Nibbs R.J.B., Graham G.J. (2013) Immune regulation by atypical chemokine receptors. *Nature Reviews Immunology* **2013** *13*:11 **13**:815-829 <https://doi.org/10.1038/nri3544> | PubMed
- [25] Gosling J., Dairaghi D.J., Wang Y., Hanley M., Talbot D., Miao Z., Schall T.J. (2000) Cutting Edge: Identification of a Novel Chemokine Receptor That Binds Dendritic Cell- and T Cell-Active Chemokines Including ELC, SLC, and TECK. *The Journal of Immunology* **164** <https://doi.org/10.4049/JIMMUNOL.164.6.2851> | PubMed

- [26] Zhou A.L., Jensen D.R., Peterson F.C., Thomas M.A., Schlimgen R.R., Dwinell M.B., Smith B.C., Volkman B.F. (2023) Fragment-based drug discovery of small molecule ligands for the human chemokine CCL28. *SLAS Discovery* **28**:163-169 <https://doi.org/10.1016/j.slasd.2023.02.004> | PubMed
- [27] Jumper J., Evans R., Pritzel A., Green T., Figurnov M., Ronneberger O., Tunyasuvunakool K., Bates R., Židek A., Potapenko A., et al. (2021) Highly accurate protein structure prediction with AlphaFold. *Nature* **2021** **596**:583-589 <https://doi.org/10.1038/s41586-021-03819-2> | PubMed
- [28] Fox D.R., Taveneau C., Clement J., Grinter R., Knott G.J. (2025) Code to complex: AI-driven de novo binder design. *Structure* **33**:1631-1642 <https://doi.org/10.1016/j.str.2025.08.007> | PubMed
- [29] Team C.D., Boitreau J., Dent J., Geisz D., McPartlon M., Meier J., Qiao Z., Rogozhnikov A., Rollins N., Wollenhaupt P., et al. (2025) Zero-shot antibody design in a 24-well plate. *BioRxiv* <https://doi.org/10.1101/2025.07.05.663018>
- [30] Zambaldi V., La D., Chu A.E., Patani H., Danson A.E., Kwan T.O.C., Frerix T., Schneider R.G., Saxton D., Thillaisundaram A., et al. (2024) De novo design of high-affinity protein binders with AlphaProteo. *arXiv* <https://doi.org/10.48550/arxiv.2409.08022>
- [31] Pacesa M., Nickel L., Schellhaas C., Schmidt J., Pyatova E., Kissling L., Barendse P., Choudhury J., Kapoor S., Alcaraz-Serna A., et al. (2025) One-shot design of functional protein binders with BindCraft. *Nature* **646**:483-492 <https://doi.org/10.1038/s41586-025-09429-6> | PubMed
- [32] Evans R., O'Neill M., Pritzel A., Antropova N., Senior A., Green T., Židek A., Bates R., Blackwell S., Yim J., et al. (2022) Protein complex prediction with AlphaFold-Multimer. *BioRxiv* <https://doi.org/10.1101/2021.10.04.463034>
- [33] Goverde C.A., Pacesa M., Goldbach N., Dornfeld L.J., Balbi P.E.M., Georgeon S., Rosset S., Kapoor S., Choudhury J., Dauparas J., et al. (2024) Computational design of soluble and functional membrane protein analogues. *Nature* **631**:449-458 <https://doi.org/10.1038/s41586-024-07601-y> | PubMed
- [34] Leman J.K., Weitzner B.D., Lewis S.M., Adolf-Bryfogle J., Alam N., Alford R.F., Aprahamian M., Baker D., Barlow K.A., Barth P., et al. (2020) Macromolecular modeling and design in Rosetta: recent methods and frameworks. *Nat. Methods* **17**:665-680 <https://doi.org/10.1038/s41592-020-0848-2> | PubMed
- [35] Filius M., Patsos T., Minnee H., Turco G., Chong H.E., Liu J., Gnatzy M., Rooth R.S.M., Liu A.C.H., Ta R.D.T., et al. (2025) Evaluating BindCraft for Generative Design of High-Affinity Peptides. *ACS Chem. Biol* <https://doi.org/10.1021/ACSCHEMBIO.5C00774> | PubMed
- [36] Smith E.W., Nevins A.M., Qiao Z., Liu Y., Getschman A.E., Vankayala S.L., Kemp M.T., Peterson F.C., Li R., Volkman B.F., et al. (2016) Structure-Based Identification of Novel Ligands Targeting Multiple Sites within a Chemokine-G-Protein-Coupled-Receptor Interface. *J. Med. Chem* **59**:4342-4351 <https://doi.org/10.1021/ACSJMEDCHEM.5B02042> | PubMed
- [37] Ber oni D., Tsenko M., Mag ana P., Nair S., Pidruc hna I. anna, Af onso M. celo Querino Lima, dam Midlik A., mila aramv al U.P., La al D., Tan eer A., et al. (2013) AlphaFold Protein Structure Database 2025: a redesigned interface and updated structural coverage. *Nucleic Acids Res.* **1**:13-14 <https://doi.org/10.1093/NAR/GKAF1226> | PubMed
- [38] Valdés-Tresanco M.S., Valdés-Tresanco M.E., Valiente P.A., Moreno E. (2021) gmx_MMPBSA: A New Tool to Perform End-State Free Energy Calculations with GROMACS. *J. Chem. Theory Comput* **17**:6281-6291 <https://doi.org/10.1021/ACS.JCTC.1C00645> | PubMed
- [39] Abramson J., Adler J., Dunger J., Evans R., Green T., Pritzel A., Ronneberger O., Willmore L., Ballard A.J., Bambrick J., et al. (2024) Accurate structure prediction of biomolecular interactions with AlphaFold 3. *Nature* **630**:493-500 <https://doi.org/10.1038/s41586-024-07487-w> | PubMed
- [40] Watts A.O., Verkaar F., Van Der Lee M.M.C., Timmerman C.A.W., Kuijjer M., Van Offenbeek J., Van Lith L.H.C.J., Smit M.J., Leurs R., Zaman G.J.R., et al. (2013) β -Arrestin Recruitment and G Protein Signaling by the Atypical Human Chemokine Decoy Receptor CCX-CKR. *Journal of Biological Chemistry* **288**:7169-7181 <https://doi.org/10.1074/JBC.M112.406108> | PubMed
- [41] Lamme T.D., Smit M.J., Schafer C.T. (2025) Signal termination of the chemokine receptor CCR9 is governed by an arrestin-independent phosphorylation mechanism. *Journal of Biological Chemistry* **301** <https://doi.org/10.1016/j.jbc.2025.108462> | PubMed

- [42] Wan Q., Okashah N., Inoue A., Nehme R., Carpenter B., Tate C.G., Lambert N.A. (2018) Mini G protein probes for active G protein-coupled receptors (GPCRs) in live cells. *J. Biol. Chem* **293**:7466-7473 <https://doi.org/10.1074/JBC.RA118.001975> | PubMed
- [43] Namkung Y., Le Gouill C., Lukashova V., Kobayashi H., Hogue M., Khoury E., Song M., Bouvier M., Laporte S.A. (2016) Monitoring G protein-coupled receptor and β -arrestin trafficking in live cells using enhanced bystander BRET. *Nat. Commun* **7** <https://doi.org/10.1038/NCOMMS12178> | PubMed
- [44] Uhlen M., Karlsson M.J., Zhong W., Tebani A., Pou C., Mikes J., Lakshminanth T., Forsström B., Edfors F., Odeberg J., et al. (2019) A genome-wide transcriptomic analysis of protein-coding genes in human blood cells. *Science (1979)* **366** <https://doi.org/10.1126/SCIENCE.AAX9198> | PubMed
- [45] Cao Y., Zhang C., Yuan Q., Zhao F., Liu Q., Wu K., Hu W., He J., Li H., Xu H.E., et al. (2025) Mechanisms of chemokine recognition and receptor activation of chemokine receptor CCR7. *Cell Rep* **44** <https://doi.org/10.1016/J.CELREP.2025.116582> | PubMed
- [46] Bekker P., Ebsworth K., Walters M.J., Berahovich R.D., Ertl L.S., Charvat T.T., Punna S., Powers J.P., Campbell J.J., Sullivan T.J., et al. (2015) CCR9 Antagonists in the Treatment of Ulcerative Colitis. *Mediators Inflamm* <https://doi.org/10.1155/2015/628340> | PubMed
- [47] Zhang J., Romero J., Chan A., Goss J., Stucka S., Cross J., Chamberlain B., Varoglu M., Chandonnet H., Ryan D., et al. (2015) Biarylsulfonamide CCR9 inhibitors for inflammatory bowel disease. *Bioorg. Med. Chem. Lett* **25**:3661-3664 <https://doi.org/10.1016/J.BMCL.2015.06.046> | PubMed
- [48] Anishchenko I., Pellock S.J., Chidyausiku T.M., Ramelot T.A., Ovchinnikov S., Hao J., Bafna K., Norn C., Kang A., Bera A.K., et al. (2021) De novo protein design by deep network hallucination. *Nature* **600**:547-552 <https://doi.org/10.1038/s41586-021-04184-w> | PubMed
- [49] Kortemme T. (2024) De novo protein design—From new structures to programmable functions. *Cell* **187**:526-544 <https://doi.org/10.1016/J.CELL.2023.12.028> | PubMed
- [50] De Magalhaes Pinheiro I., Dawson J.R.D., Calo N., Paolini-Bertrand M., Akondi K.B., Tan G., Handel T.M., Kufareva I., Hartley O. (2025) Noncanonical roles of chemokine regions in CCR9 activation revealed by structural modeling and mutational mapping. *Nat. Commun* **16** <https://doi.org/10.1038/s41467-025-62321-9> | PubMed
- [51] Drurya L.J., Ziarek J.J., Gravel S., Veldkamp C.T., Takekoshi T., Hwang S.T., Heveker N., Volkman B.F., Dwinell M.B. (2011) Monomeric and dimeric CXCL12 inhibit metastasis through distinct CXCR4 interactions and signaling pathways. *Proc. Natl. Acad. Sci. U. S. A* **108**:17655-17660 <https://doi.org/10.1073/pnas.1101133108> | PubMed
- [52] Zhang Y., Skolnick J. (2005) TM-align: a protein structure alignment algorithm based on the TM-score. *Nucleic Acids Res* **33**:2302-2309 <https://doi.org/10.1093/NAR/GKI524> | PubMed
- [53] McInnes L., Healy J., Melville J. (2018) UMAP: Uniform Manifold Approximation and Projection for Dimension Reduction. *Journal of Open Source Software* **3**:861 <https://doi.org/10.21105/joss.00861>
- [54] Bouysset C., Fiorucci S. (2021) ProLIF: a library to encode molecular interactions as fingerprints. *Journal of Cheminformatics* **13**:72 <https://doi.org/10.1186/S13321-021-00548-6> | PubMed
- [55] Lee J., Cheng X., Swails J.M., Yeom M.S., Eastman P.K., Lemkul J.A., Wei S., Buckner J., Jeong J.C., Qi Y., et al. (2015) CHARMM-GUI Input Generator for NAMD, GROMACS, AMBER, OpenMM, and CHARMM/OpenMM Simulations Using the CHARMM36 Additive Force Field. *J. Chem. Theory Comput.* **12**:405-413 <https://doi.org/10.1021/ACS.JCTC.5B00935> | PubMed
- [56] Huang J., Rauscher S., Nawrocki G., Ran T., Feig M., De Groot B.L., Grubmüller H., MacKerell A.D. (2016) CHARMM36m: an improved force field for folded and intrinsically disordered proteins. *Nat. Methods* **14**:71-73 <https://doi.org/10.1038/nmeth.4067> | PubMed
- [57] Van Der Spoel D., Lindahl E., Hess B., Groenhof G., Mark A.E., Berendsen H.J.C. (2005) GROMACS: Fast, flexible, and free. *J. Comput. Chem.* **26**:1701-1718 <https://doi.org/10.1002/jcc.20291> | PubMed
- [58] Bussi G., Donadio D., Parrinello M. (2007) Canonical sampling through velocity rescaling. *Journal of Chemical Physics* **126**:14101 <https://doi.org/10.1063/1.2408420>

- [59] Bernetti M., Bussi G. (2020) Pressure control using stochastic cell rescaling. *Journal of Chemical Physics* **153**:114107 <https://doi.org/10.1063/5.0020514>
- [60] Michaud-Agrawal N., Denning E.J., Woolf T.B., Beckstein O. (2011) MDAAnalysis: A toolkit for the analysis of molecular dynamics simulations. *J. Comput. Chem* **32**:2319-2327 <https://doi.org/10.1002/JCC.21787> | PubMed
- [61] Valdés-Tresanco M.S., Valdés-Tresanco M.E., Valiente P.A., Moreno E. (2021) gmx_MMPBSA: A New Tool to Perform End-State Free Energy Calculations with GROMACS. *J. Chem. Theory Comput* **17**:6281-6291 <https://doi.org/10.1021/ACS.JCTC.1C00645> | PubMed
- [62] Abramson J., Adler J., Dunger J., Evans R., Green T., Pritzel A., Ronneberger O., Willmore L., Ballard A.J., Bambrick J., et al. (2024) Accurate structure prediction of biomolecular interactions with AlphaFold 3. *Nature* **630**:493-500 <https://doi.org/10.1038/s41586-024-07487-w> | PubMed
- [63] Bateman A., Martin M.J., Orchard S., Magrane M., Adesina A., Ahmad S., Bowler-Barnett E.H., Bye-A-Jee H., Carpentier D., Denny P., et al. (2025) UniProt: the Universal Protein Knowledgebase in 2025. *Nucleic Acids Res* **53** <https://doi.org/10.1093/NAR/GKAE1010> | PubMed
- [64] Schafer C.T., Chen Q., Tesmer J.J.G., Handel T.M. (2023) Atypical Chemokine Receptor 3 “Senses” CXC Chemokine Receptor 4 Activation Through GPCR Kinase Phosphorylation. *Mol. Pharmacol* **104**:174-186 <https://doi.org/10.1124/MOLPHARM.123.000710> | PubMed
- [65] Hunter M.R., Finlay D.B., Macdonald C.E., Cawston E.E., Grimsey N.L., Glass M. (2017) Real-Time Measurement of Cannabinoid Receptor-Mediated cAMP Signaling. *Methods Enzymol* **593**:43-59 <https://doi.org/10.1016/BS.MIE.2017.05.001> | PubMed
- [66] Roy S., Sinha S., Silas A.J., Ghassemian M., Kufareva I., Ghosh P. (2024) Growth factor-dependent phosphorylation of Gai shapes canonical signaling by G protein-coupled receptors. *Sci. Signal* **17** <https://doi.org/10.1126/scisignal.ade8041> | PubMed
- [67] Gustavsson M., Zheng Y., Handel T.M. (2016) Production of Chemokine/Chemokine Receptor Complexes for Structural Biophysical Studies. *Methods Enzymol* **570**:233-260 <https://doi.org/10.1016/BS.MIE.2015.10.003> | PubMed

Peer reviews

Reviewer #1 (Public review):

Summary:

In this manuscript, the authors describe the use of BindCraft computational protein design to create a series of binders to the chemokine CCL25. This chemokine normally mediates CCR9-dependent trafficking of immune cells to the gut, making it a potential target for the treatment of inflammatory bowel disease and related conditions. Importantly, CCL25 also binds a scavenging receptor, ACKR4. The computational protein design approach used does not involve defining particular epitopes to be targeted, allowing a free search for any potential interaction surface.

Among four designs tested, three were predicted to interact at a similar site on the chemokine, while a fourth clone, VUP25111, was predicted to bind to a different site. All four designs showed binding to CCL25, with similar high-nM KD values in all cases. The first three clones showed evidence of direct competition with the receptor for CCL25 binding, while VUP25111 showed incomplete inhibition of binding. In functional assays, all clones acted as antagonists except for VUP25111, which inhibited arrestin recruitment by CCR9, but did not affect G protein activation by CCR9 or arrestin recruitment by ACKR4 (which signals exclusively through arrestin and not G protein).

Strengths:

The work is completed to a high technical standard, and the functional diversity of the clones is intriguing. It is exciting to see pathway-selective modulation of signaling, and this basic paradigm is likely to generalize to other chemokine/receptor systems. The exceptional complexity of chemokine signaling makes this an excellent area to explore the development of modulators that can restrict signaling to a specific subset of receptors.

Weaknesses:

No major weaknesses were noted by this reviewer.

<https://doi.org/10.7554/eLife.111190.1.sa3>

Reviewer #2 (Public review):

This study from de Boer, Lamme, Verdwaald and Schafer describes the de novo AI-guided design of miniproteins that target the chemokine CCL25, with the aim to modulate the activation and signalling of the chemokine receptors CCR9 and ACKR4. The study focuses on characterising four miniproteins that all bind CCL25 with good affinity. Three designs appear to prevent CCL25 binding to both CCR9 and ACKR4, with increasing concentrations of miniproteins resulting in decreased arrestin (both receptors) and mini G protein recruitment (CCR9), less inhibition of forskolin-stimulated cAMP (CCR9), and decreased GRK3 recruitment and receptor internalisation (CCR9). One miniprotein, VUP25111, changes the properties of CCL25 rather than preventing ligand/receptor interactions, resulting in greater selectivity for CCR9 over ACKR4 and a G protein-biased signalling profile (maintenance of mini G protein recruitment, GRK3 recruitment, inhibition of cAMP and receptor internalisation, but loss of arrestin recruitment). VUP25111 also maintained chemotactic migration in MOLT-4 T lymphoblast cells, whereas this response was lost in the presence of the other three miniproteins.

Overall, this is a very interesting application of AI-designed de novo miniproteins to modulate GPCR responses by directly binding the ligand rather than the receptor. This is a conceptually very intriguing approach that could, in principle, be extended to other GPCR systems beyond the chemokine family. The authors deploy an impressive array of assays spanning multiple signalling endpoints, providing a thorough picture of how each miniprotein influences receptor activation and downstream signalling. The presentation of concentration-response relationships for CCL25 alone and in the presence of each miniprotein is particularly informative, and the figures are very well constructed throughout. The inclusion of clear cartoons illustrating the basis of each assay is a nice touch that will help readers from outside the immediate field follow the logic of each experiment.

There are two main conclusions that are not currently as well-supported by the evidence as they might be, and that would benefit from some qualification. The first concerns the selectivity of the miniproteins for CCL25. Testing the impact of the miniproteins on CXCL12 activation of CXCR4 is an important and welcome experiment, but it addresses selectivity against only one other chemokine system, and the current claim of specificity is therefore stronger than the data allow. Additionally, at the highest concentration tested (10 μ M), the more potent miniproteins (VUP25101, VUP25107) appear to show some inhibition of arrestin recruitment to CXCR4 - perhaps unsurprising given the degree of structural conservation among chemokines. The statements regarding selectivity and the lack of effect on the CXCL12/CXCR4 system would benefit from revision to more accurately reflect these observations.

The second concern relates to the interpretation of the preserved GRK3 recruitment, but the complete loss of arrestin recruitment observed with VUP25111. In the GRK3 recruitment experiments, 20 nM CCL25 was used, representing an EC40 concentration in this assay. VUP25111 causes a concentration-dependent reduction in CCL25-induced GRK3 recruitment,

down to approximately 15% of the maximal response. It is worth considering whether this degree of reduction in GRK3 recruitment could itself be sufficient to disrupt patterns of receptor phosphorylation and thereby prevent observable arrestin recruitment. Both interpretations are complicated by the fact that the GRK3 recruitment and arrestin recruitment assays likely differ in their sensitivity and dynamic windows, making direct quantitative comparisons between them difficult. In the absence of direct measurements of CCR9 phosphorylation in the presence of VUP25111, the alternative interpretation remains open and would benefit from acknowledgement. Given recent work from the same group demonstrating that receptor internalisation is only partially dependent on arrestins (Lamme et al., 2025, *J Biol Chem*), further discussion of the relationship between GRK and arrestin recruitment and CCR9 internalisation would be of value to the broader GPCR audience this work is likely to attract.

Finally, some additional justification for the use of 20 nM CCL25 across all assays would strengthen the study, as this concentration represents different points on the concentration-response curve depending on the assay and receptor in question. It ranges from an EC40 for CCR9 GRK3 recruitment and internalisation, to an EC50 for CCR9 arrestin and mini-Gi recruitment, an EC80 for CCR9 cAMP inhibition, and an EMax for ACKR4 arrestin recruitment. This has potential consequences for the interpretation and cross-assay comparison of miniprotein potency, and the authors are encouraged to acknowledge and discuss this in the context of their conclusions.

<https://doi.org/10.7554/eLife.111190.1.sa2>

Reviewer #3 (Public review):

Summary:

The authors employed the BindCraft platform to develop binders targeting the chemokine CCL25, a selective activator of the chemokine receptor CCR9. They successfully generated two classes of binders: one that inhibits all CCL25-mediated CCR9 activation, and another that permits CCR9 G protein signaling while simultaneously preventing arrestin recruitment. These tools will enable the dissection of arrestin involvement in regulating cell migration.

My comments, in the order of reading:

(1) Title: I strongly recommend removing the term "biasing" from the title. In this context, it does not convey a specific mechanistic concept. The term "biased signaling" has been used for a very broad range of mechanistically distinct pharmacological phenomena, and without a precise definition, it adds more confusion than clarity. I therefore suggest refraining from using it in the title.

(2) Abstract, line 34: The term "bias" should be replaced. As currently used, it appears to suggest a dichotomy between G protein signaling and arrestin recruitment. However, arrestin recruitment is a consequence of G protein signaling, and it is not conceptually sound to compare a signaling event mediated by one protein family with a protein-protein interaction involving another protein family. A meaningful comparison requires experimental paradigms that differ by a single variable; in this case, there are two - distinct protein families and fundamentally different types of readouts (signaling versus protein-protein interaction).

(3) Abstract, line 34: The term "balanced agonist" should be removed. Any chosen reference ligand is, by definition, the "balanced" agonist for that analysis, regardless of its actual signaling profile. Consequently, the expression "balanced agonist" adds no mechanistic information beyond "the agonist used as reference in a particular bias calculation" and is

potentially misleading, as it implies that this ligand possesses a uniquely unbiased, system-independent signaling profile, which is not the case.

(4) Abstract, line 36: I also recommend removing the term "bias" at this point. The concept of bias typically arises from experiments that quantitatively compare more than one variable. As currently written, the phrasing suggests a dichotomy between G protein- and arrestin-mediated signaling, yet the study does not assess arrestin signaling, only arrestin recruitment. Under these conditions, the use of "bias" is not appropriate. The data are clear and compelling on their own without the need for this potentially misleading terminology.

(5) Introduction: This is interesting to read and generally well written, though certain statements would benefit from improved semantic precision. For example, in lines 110-111, the phrase "G protein-biased complex" should be reconsidered, as it relies on the notion of G protein- versus arrestin-mediated signaling. Arrestins themselves do not signal; what is measured here is their recruitment. Comparing G protein signaling with arrestin recruitment is therefore conceptually unsound, since arrestin engagement is a downstream consequence of G protein activation. Comparisons become meaningful only when designed to differentiate between G protein-dependent and G protein-independent arrestin recruitment, which is not the case in this study.

(6) Results, 122,123: The authors should consider being more precise; possibly, the truncated CCL25 is somewhat less potent on CCR9. The authors should make a statistical test and then decide whether to rephrase or not for enhanced precision.

(7) Figure S5: This figure is currently confusing and needs clarification. The authors state in the main text that CXCR4 is stimulated with CXCL12, yet the figure legend refers to CCL25; this discrepancy should be corrected to ensure consistency. In addition, inhibition of CXCR4 by the miniprotein binders should be analyzed and presented with normalization to CXCR4 responses, not to CCL25-stimulated CCR9. To avoid misinterpretation, inhibition by the miniproteins should be quantified separately for CCR9 and CXCR4, each normalized to its own receptor-specific and functionally equivalent stimulation condition, rather than to the "other" receptor.

(8) Results, lines 211-213: The authors should be more semantically precise. They state that no binder has any effect on arrestin recruitment to CXCR4. If I see the data, this is not really true, as 25101 and 25107 inhibit arrestin recruitment by about 50 % or more at the highest applied concentrations; only 111 and 112 are completely inactive. As already commented, normalization should be done to arrestin recruitment of CXCR4 and not CCR9.

<https://doi.org/10.7554/eLife.111190.1.sa1>

Author response:

We thank the editors and reviewers for thoroughly reviewing our manuscript and offering thoughtful and constructive feedback. We appreciate the positive reception of our work and welcome the opportunity to address the lingering concerns. In the coming revisions, we will be directly addressing the question of the miniprotein's specificity and increase the precision in the language used to discuss our findings.

<https://doi.org/10.7554/eLife.111190.1.sa0>